Faraday Discussions

Cite this: DOI: 10.1039/d5fd00110b

PAPER

Spiers Memorial Lecture: Multicomponent and high-entropy materials: an overview

Brian Cantor[ab]

Received 1st September 2025, Accepted 9th September 2025
DOI: 10.1039/d5fd00110b

Multicomponent phase space is enormous and contains a vast number of complex new materials. Despite intensive investigation in the last decade and a half however, we are only slowly making progress towards understanding these new materials. This paper attempts to summarise some of the fundamental discoveries we have made about the geography of multicomponent phase space and the wide range of complex new materials that we have found within it. This paper discusses briefly the following topics: the size and shape of multicomponent phase space and the range of single- and multiple-phase fields that it contains; the (initially) surprising presence of many large near-ideal single-phase solid-solution phases, stabilised by a high configurational entropy of mixing; the extensive and wide-ranging variation of local nanostructure and associated mechanical and electronic lattice strain that permeates throughout high-entropy solid-solution phases; and some of the unusual, exciting and valuable properties that are then produced within multicomponent and high-entropy materials. Many of the results discussed have been obtained from the fcc Cantor alloys (based on the original Cantor alloy, equiatomic fcc CrMnFeCoNi) and the bcc Senkov alloys (based on the original Senkov alloy, equiatomic VNbMoTaW), two groups of multicomponent high-entropy single-phase materials that have been particularly widely studied. Similar behaviour is also found in other multicomponent high-entropy single-phase materials, though these have not been studied so intensively. In comparison with multicomponent high-entropy single-phase materials, rather little is known about multicomponent multiphase materials that have also not been studied so intensively.

[a]*Department of Materials, University of Oxford, Parks Road, Oxford OX1 3PH, UK. E-mail: brian.cantor@materials.ox.ac.uk*

[b]*Brunel Advanced Solidification Centre (BCAST), Brunel University London, Uxbridge, UB8 3PH, UK. E-mail: brian.cantor@brunel.ac.uk*

1. Introduction

All materials are alloys.†[1,2] This is sometimes for the negative reason that we can never manufacture perfectly pure materials without retaining small admixtures of impurities (a consequence of the third law of thermodynamics), but it is more often for the more positive reason that we frequently add alloying elements to obtain secondary properties in a material or to tweak the primary properties of its main component. Until recently almost all the materials we have made and used have been composed of one or occasionally two main components and a relatively small number of relatively low-level dilute alloying additions.[1–3] In 1979, I invented the concept of multicomponent materials,‡ *i.e.* materials with more (and often many more) than two components in relatively concentrated proportions,[3–5] and the first experiments to investigate multicomponent materials were performed in 1980 under my supervision by an undergraduate student, Alain Vincent, for his short 2nd-year undergraduate project at the

† This paper uses the term alloy to mean any mixture of more than one starting material or component. The term alloy is used most commonly to refer to metallurgical materials, but here it is used more generally for any mixture of materials, whether metallurgical, ceramic, semiconductor, polymeric or of any other type. Since all materials are alloys, as explained in the main text, the two terms material and alloy are fairly synonymous but not entirely, since referring to different alloys usually means referring (only) to different compositions of the mixed components, whereas referring to different materials often means referring to different compositions, but can also mean referring to the same composition made under different manufacturing conditions and with different resulting microstructures. Thus, for instance, martensitic and ferritic steels with the same composition are the same alloy but different materials; and, similarly, amorphous and devitrified soda-lime glasses with the same composition are also the same alloy but different materials.

† This paper uses the term alloy to mean any mixture of more than one starting material or component. The term alloy is used most commonly to refer to metallurgical materials, but here it is used more generally for any mixture of materials, whether metallurgical, ceramic, semiconductor, polymeric or of any other type. Since all materials are alloys, as explained in the main text, the two terms material and alloy are fairly synonymous but not entirely, since referring to different alloys usually means referring (only) to different compositions of the mixed components, whereas referring to different materials often means referring to different compositions, but can also mean referring to the same composition made under different manufacturing conditions and with different resulting microstructures. Thus, for instance, martensitic and ferritic steels with the same composition are the same alloy but different materials; and, similarly, amorphous and devitrified soda-lime glasses with the same composition are also the same alloy but different materials.

‡ This paper draws a distinction between multicomponent and high-entropy materials. The term "multicomponent material" is taken to mean any material containing three or more components, *i.e.* with $c \geq 3$, where c is the number of components in the material. This is logical and natural, in line with the normal definition of multiple as meaning more than one or two. The term high-entropy material is more restrictive and is taken to mean any multicomponent material, *i.e.* any material containing three or more components with $c \geq 3$, where in addition the components are all or almost all in one or, at most, two random or near-random solid-solution phases. This is again more logical and natural, in line with the implied normal definition of high entropy as meaning a configurational entropy of mixing in the material sufficiently large to stabilise one or at most two random solid-solution phases, rather than forming a mixture of several or many stoichiometric, fixed-composition or near-fixed-composition compounds. This is different, but simpler and less arbitrary, than the common usage of the terms high-entropy material and medium-entropy material to mean any material containing high concentrations of more than five components, *i.e.* $c \geq 5$, and between three and five components, *i.e.* $5 \geq c \geq 3$, respectively. Overall the definitions used in this paper are, as already indicated, more logical and more natural than some common practice, and also more useful, since they carefully separate the different concepts of multiplicity of components and entropy in any given material.

University of Sussex.[3–5] These first experiments led almost immediately to the discovery of a number of interesting multicomponent materials, including the first high-entropy material, the original Cantor alloy,§ consisting of five components (Cr, Mn, Fe, Co and Ni) in equal proportions, with a single-phase random solid-solution face-centred cubic (fcc) crystal structure, which can be represented more succinctly as fcc CrMnFeCoNi.¶ These studies were reported in Vincent's undergraduate project dissertation[5] at the University of Sussex, but, although the results were indisputable and very clear, they were not of the quality needed to be accepted by a research journal for publication. For complex reasons, it was a long time before the work could be repeated, so the results were not fully published until more than twenty years later. The multicomponent material concept was first published, therefore, in 2002 and 2003, when it was mentioned briefly in the introduction to several papers by myself with other colleagues on some multicomponent amorphous alloys,[6–9] work that was performed in the early 2000s, *i.e.* much later than the original work by Vincent. The original work was finally published in our seminal paper[4] expounding the details of the new concept in 2004. In the meantime, Jien-Wei Yeh in Taiwan had quite independently had similar ideas to me and had pursued similar experiments in the mid-1990s, and he and his colleagues had also discovered immediately a variety of interesting multicomponent materials that he at first called multiple-principal-element materials. This work also took some time (though not quite so long) before it was finally published in four papers,[10–13] again in 2004. In one of them, another seminal paper[11] again expounding the details of the new concept, he invented the alternative name high-entropy materials that has been used widely (and somewhat confusingly, as explained in a previous footnote and in a later section) for the whole field of multicomponent materials.

There was antipathy and some disdain amongst scientific colleagues and research funders in the 1980s, 1990s and 2000s about the idea of investigating multicomponent and high-entropy materials, and Yeh and myself both received considerable resistance from our respective academic establishments against pursuing our early experiments, which partly explains the lengthy delays in both cases between our first research work being undertaken and then finally being published.[14,15] For similar reasons, our first published papers on multicomponent and high-entropy materials in the early 2000s, including the two seminal papers

§ The term Cantor alloy means any multicomponent material with a single-phase random or near-random solid-solution face-centred cubic (fcc) structure. There are very many Cantor alloys with different compositions, as discussed later in the main text.

¶ This paper adopts the convention of naming multicomponent and high-entropy materials by listing their components in ascending atomic number rather than alphabetically, *i.e.* the original Cantor alloy is represented as CrMnFeCoNi rather than CoCrFeMnNi. This has the advantage of emphasising more clearly the chemical nature of the different components. This paper also adopts the convention of naming multicomponent and high-entropy materials by using subscripts for the atomic percent rather than weight percent of the different components, but truncated by leaving out the subscripts when the components are present in equiatomic proportions, *i.e.* the original Cantor alloy is represented as CrMnFeCoNi, truncated from $Cr_{20}Mn_{20}Fe_{20}Co_{20}Ni_{20}$. The paper deviates from the ascending atomic number convention when it contradicts a well-established usage. Thus, the well-known and important ordered body-centred cubic (bcc) multicomponent monoaluminide is represented as (CrMnFeCoNi)Al rather than Al(CrMnFeCoNi).

mentioned above, did not initially receive much (or even any) significant scientific attention, with only a few citations in the first five or ten years following their publication. Since then, however, scientific interest has mushroomed rapidly, with citations increasing dramatically and multi-million dollar research programmes being initiated in many countries worldwide.[3,16,17] The discovery of multicomponent high-entropy materials has opened up the possibility of developing many new materials with exciting new properties and, after an initial delay, scientists have, not surprisingly, begun to realise their potential and have been increasingly active in investigating different multicomponent materials and trying to understand their structures and properties.[3,16] The Web of Science gives a total, up to the present time, of almost fifty thousand research papers on multicomponent or high-entropy alloys or materials, and Google Scholar gives a total of approximately ten and fifteen thousand citations, respectively, for each of the two seminal papers by Cantor and Yeh mentioned above. And the number of scientific papers on multicomponent materials and the number of citations to them are both continuing to rise rapidly.

The last decade and a half in the 2010s and 2020s has seen, therefore, a fairly large body of scientific investigation into the manufacture and resulting structures and properties of multicomponent and high-entropy materials.[3,16,17] It turns out, however, that multicomponent phase space is vast, and contains a truly enormous number of materials, running into many trillions, the majority of which have still never been made, let alone investigated in any detail.[3,16,17] Until we began to study multicomponent materials seriously in the 2010s and 2020s, virtually all the materials that we had ever made had been based, as mentioned above, on either a single component or binary mixtures of different components, with only occasionally a concentrated ternary addition, and with higher order (quaternary, quinary, *etc.*) additions never much above very dilute levels. To put it another way, all our materials have until recently been at or very close to the corners and binary edges and occasionally the ternary faces of multicomponent phase space, and we have until recently avoided exploring the inner regions within the main body of multicomponent phase space where most of the compositions of the trillions of different and new multicomponent materials can be found. Unfortunately, it also turns out that our thermodynamic, classical and quantum mechanical, and statistical theories of the structure and properties of materials have all been devised for relatively pure materials and/or simple mixtures with only one or two relatively dilute alloying additions that can then be treated as relatively small and independent linear perturbations of the properties of the main component in the material.[3,18] Because of the approximations required to make these theories tractable as well as the multiplicity of parameters needed to make calculations based on them, our fundamental theories are not easily extrapolated to the complexity of multicomponent materials, which often exhibit non-linear behaviour because of the interactions between multiple components in concentrated proportions.[3,18] This means that in order to explore multicomponent phase space and the different materials within it, there is no real alternative to massive amounts of experimental investigation to provide new data that will ultimately allow us to develop more complex and more definitive theories of multicomponent material structures and properties. At present, however, the size of multicomponent phase space is so large that, despite

intensive research over the last decade and a half, we have still explored only a small fraction of the totality of all possible materials that could be made, so we are still a long way from developing a detailed scientific understanding of the range and extent of all the different multicomponent materials and their structures and properties.[3,18]

Despite these difficulties, after considerable false starts and with considerable initial misunderstandings, we have finally begun to understand some of the main features of the geography of multicomponent phase space and of the structures and properties of some of the different multicomponent materials within it,[3,16,17] and it is the purpose of this paper to try to summarise briefly where we have got to. I do this by asking a series of simple and obvious questions (that I am frequently asked) and either giving the answer or answers that we have finally been able to come up with, often after a lot of hard work to clear away initial misconceptions, or alternatively indicating the extent of our continued lack of understanding and the need for further work (a conclusion that is still fairly common, essentially because of the enormity of multicomponent phase space and the complexity of the structure and properties of the multicomponent materials within it).

2. How many materials are there?

The number of materials we can make depends firstly on the number of starting materials or components c that we have available, and secondly on the material specification x, *i.e.* the difference in composition that separates two similar but different materials. For a material specification x in at% or mole%, there are $n = 100/x$ different compositions available for each of the components in the material. The specification x is important[19–21] in defining the range of compositions within which a given material can vary and can still be regarded as the same material with a specified structure and properties. The specification reflects the precision within which we can manufacture a material, as well as the precision we need for its application.[19–21] Anyone making a material needs to know how tightly the composition must be controlled during manufacture, and anyone using a material needs to know that they have the correct material composition within this range and thus the correct specified properties. We can think of the totality of multicomponent phase space as being represented by a c-pointed hyper-polyhedron in $(c - 1)$-dimensional hyperspace with the number of different materials within it being given by the number of composition points separated by x at% along each of the c polyhedral axes (*i.e.* analagous to a three-pointed polyhedron (a triangle) as is used in two-dimensional space (on the page) to represent a conventional ternary alloy system).[3]

Calculating the total number of materials in a given alloy system is a matter of combinatorial maths.[22,23] If one out of $n = 100/x$ atoms is changed from one kind to another, the composition changes by x at%, the material goes out of specification, and it is effectively changed into a different material. We need, therefore, to work out how many different ways we can pick $n = 100/x$ atoms from c different kinds of atom (*i.e.* c different components), with the order of picking being irrelevant, *i.e.* mathematically a combination rather than a permutation, and with multiple picking of atoms of each type allowed, *i.e.* mathematically with repetition rather than without repetition. For c components and $n = 100/x$ composition

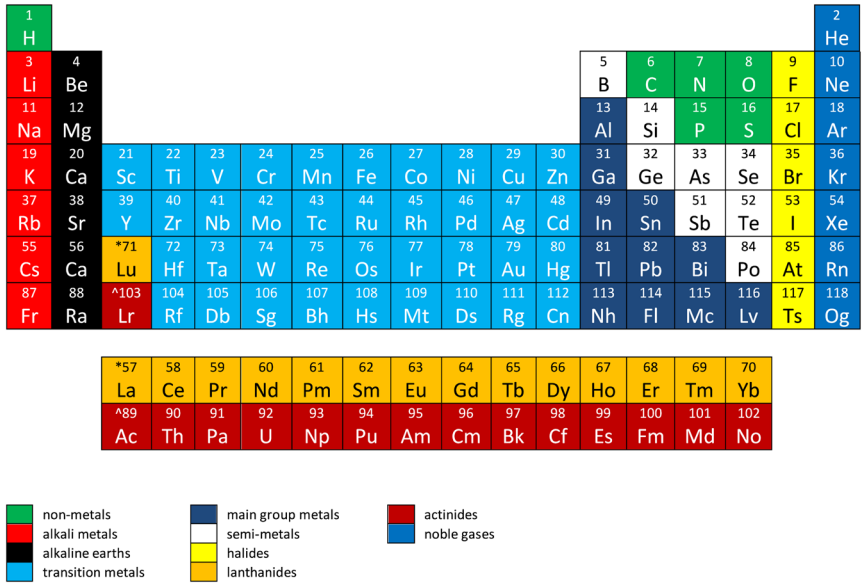

Fig. 1 The periodic table.

Table 1 The number of different materials N, in the form $\log_{10}(N)$, that can be manufactured from c components, with a material specification of x at%, corresponding to a number of composition points $n = 100/x$ for each component

x (at%)	n	$c = 40$	$c = 50$	$c = 60$	$c = 70$	$c = 80$
5	20	16	18	19	21	22
1	10^2	36	41	46	50	53
0.1	10^3	72	86	100	111	123
0.01	10^4	111	134	157	179	200
0.001	10^5	150	183	216	248	279

points for each component, the total number of materials that can be made N is given then by the law of combinations with repetition:[22,23]

$$N = \binom{c+n-1}{n} = \frac{(c+n-1)!}{(c-1)!n!}$$
$$= \exp\{(c+n-1)\ln(c+n-1) - (c-1)\ln(c-1) - n\ln n\}$$

where the first expression on the right-hand side uses the bracket notation for a binomial coefficient, and the last expression comes from using Stirling's approximation for large numbers.

We can generate the whole of multicomponent phase space, containing all the possible materials that could conceivably be made, by using all the elements in the periodic table, shown in Fig. 1, as our set of starting materials or components. This gives us a total of $c = 118$ components with which to manufacture different materials. We can reduce this to $c = 80$, by removing all the elements in row seven

because they are radioactive with short lifetimes, and also removing all the elements in column eighteen because they are noble gases and chemically inert. Alternatively, we might want to be more restrictive and take (say) $c = 50$ or 60, because some of the remaining elements are highly reactive and difficult to handle, such as lithium, fluorine or arsenic, though all these elements are used in important materials. Most engineering materials are specified to $x = 0.1\%$, though lower-grade materials are often specified to no better than $x = 1\%$ or 5%, and some high-performance materials require a greater degree of specification, down to $x = 0.01\%$, or 0.001%[19–21] (or even, in some special cases, to the nearest part per million (ppm) or $x = 0.0001\%$).

Table 1 shows the total number of materials that can be made using different assumptions for the number of components c, the specification x, and the number of composition points for each component $n = 100/x$. Taking $c = 80$, $x = 0.1\%$ and $n = 1000$ gives the total number of materials that can be made as:

$$\ln N = 1079 \ln 1079 - 79 \ln 79 - 1000 \ln 1000 \approx 282$$

$$\therefore N = 10^{123}$$

Being extremely conservative and taking $c = 60$ and $x = 1\%$ or even 5% gives the total number of materials that can be made as $N = 10^{46}$ or 10^{19} respectively. In all cases, the number of possible materials that could be made is enormous. Many multicomponent material compositions will, of course, be difficult to manufacture and not be of much use. Nevertheless, it is quite clear that, whatever values are used for c, x and n, there is an extremely large number of different materials populating multicomponent phase space.

3. Are multicomponent materials the same as high-entropy materials?

The terms multicomponent materials (first used by me and my colleagues), multiple-principal-element materials, and high-entropy materials (both first used by Yeh and his colleagues) have often been used to mean the same thing.[3,16,17] This is misleading and somewhat confusing. I prefer to use multicomponent materials to mean all materials with more than one or two components, *i.e.* with $c \geq 3$; multiple-principal-element materials to mean all materials in which more than two of the components are in concentrated proportions;‖ and high-entropy materials to mean all materials in which there is an entropy sufficiently high to favour the formation of one or at most two random or near-random solid-solution phases rather than a mixture of phases that are all pure or near-pure components

‖ In this paper, the term concentrated component is taken to mean that a linear dilute solution approximation is not likely to be valid, *i.e.* that the different atoms of the component, when added in solution to the material, are not so widely separated that they can be treated as affecting the material independently or one at a time. In a solid or liquid material, atoms exhibit strong interactions chemically when they are first or second near neighbours, so a concentrated solute addition is typically above about one atom in twenty, *i.e.* >5%, depending somewhat on the structure of the host material.

and/or stoichiometric fixed-composition or near-fixed-composition compounds.** The three terms then neatly separate three different effects that can all be important independently in multicomponent materials, namely the multiplicity of the components, the concentration of the components, and the high entropy of mixing the components in a solid solution.[3] With these definitions, the set of multiple principal-element materials is a subset of the set of multicomponent materials (*i.e.* it excludes all dilute multicomponent materials), and the set of high-entropy materials is a subset of the set of multiple principal-element materials (*i.e.* it excludes all multicomponent materials where the configurational entropy is not decisive in stabilising one or at most two random solid-solution phases).

We have studied enough multicomponent materials to be able to say definitively that many but not all of them are high entropy materials.[3,16] In many cases, multicomponent materials have been found to exhibit no more than one or two random or near-random solid-solution phases:[3,16,17] in these cases, the configurational entropy of mixing is high enough to suppress chemical reactions between the different components and the resulting formation of stoichiometric fixed-composition chemical compounds. These are high-entropy materials. In many other cases, however, multicomponent materials have been found to exhibit mixtures of multiple phases:[3,16] in these cases, the configurational entropy of mixing is not high enough to suppress chemical reactions between the different components and the resulting formation of stoichiometric fixed-composition chemical compounds. These are not high-entropy materials.

4. How many high-entropy materials are there?

As explained in the last section, not all multicomponent materials are high-entropy materials, although many are. In fact, we have studied enough multicomponent materials to conclude definitively that there are often many different multicomponent materials (*i.e.* with different compositions) that have the same single-phase or multiple-phase structure (such as, for instance, single-phase fcc or two-phase fcc + bcc).[3,16] This can only happen if those particular single-phase or multiple-phase structures occupy large regions in multicomponent phase space.†† We have not yet, however, studied enough multicomponent materials to be able to map out the full extent of any of the individual multicomponent single-phase or multiple-phase fields in multicomponent phase space. We cannot yet, therefore, determine how many multicomponent materials are high-entropy materials and how many are not, though we can be sure that there are very many of each.

The Cantor alloys are the set of multicomponent materials that have a single-phase face-centred cubic (fcc) solid-solution structure, named after the first such

** In this paper, the term high-entropy material is taken to mean that the configurational entropy of the material is large enough to suppress or largely suppress the formation of stoichiometric fixed-composition compounds, leading instead to the formation of one or sometimes two extended solid-solution phases in which the atoms are randomly or near-randomly distributed across the lattice or sublattice points in the crystal structure of the material.

†† This does not mean that all single-phase or multiple-phase structures occupy large regions in multicomponent space, but we have certainly discovered that many of them do.

Table 2 Some examples of single-phase multicomponent compounds

Phase	Typical compositions
Rock salt	$(Li_{6.5}Ti_{0.5}MnNb)(O_{1.7}F_{0.3})$
	(MgCoNiCuZn)O
	(TiVZrNb)C; (TiZrNbHfTa)C
Fluorite	$(ZrYHfCe)O_2$; $(ZrYHfCeGd)O_2$
	$(TiZrSnCeHf)O_2$
	$(Mo_{0.5}CePrNdSmGd)O_2$
Pyrochlore	$(SmEuTbDyLu)_2Zr_2O_7$
	$(LaCeNdSmEu)_2Zr_2O_7$
Perovskite	$(TiMnZrSnHf)SrO_3$; $(TiGeZrSnSn)SrO_3$
	$(TiZrHfNbSn)(SrBa)O_3$
	$(YLaNdSmGd)(CrMnFeCoNi)O_3$
Spinel	$(AlMnFeCoNi)_3O_4$; $(AlCrMnFeNi)_3O_4$; $(CrMnFeCoNi)_3O_4$;
	$(CrMnFeNiZn)_3O_4$
	$(CrMnFeCoNi)Fe_2O_4$
Monoborides	(VCrNbMoTa)B; (VCrNbMoW)B (CrMnFeCoMo)B;
	(CrNiMoTaW)B
Boro-carbo-nitrides	(TiZrNbHfTa)(CN); (TiZrNbTaW)(BCN)
	(TiZrNbHfTa)(BCN); (ZrNbHfTaW)(BCN)
Hexaborides	$(YNdSmEuYb)B_6$; $(YCeSmErYb)B_6$
Disilicides	$(TiZrNbMoW)Si_2$; $(TiNbMoTaW)Si_2$

material that was discovered, the original Cantor alloy CrMnFeCoNi;[3,4,16,24] similarly, the Senkov alloys are the set of multicomponent materials that have a single-phase body-centred cubic (bcc) solid-solution structure, named after the first such material that was discovered, the original Senkov alloy VNbMoTaW.[3,16,25–27] Very many different Cantor alloys have been manufactured, probably several hundred different materials with different compositions, but all with the same single-phase fcc random or near-random solid-solution structure, and there are many more yet to be made;[3,16,24] similarly, very many different Senkov alloys have also been manufactured, again probably several hundred different materials with different compositions, but all with the same single-phase random or near-random (in this case) bcc solid-solution structure, and again there are many more yet to be made.[3,16,26,27] There have also been somewhat fewer, but still a reasonable number, of different multicomponent materials manufactured so far with different compositions but all with the same single-phase hexagonal close-packed (hcp) random or near-random solid-solution structure.[3,16] And similar behaviour has also been found in many compounds, *i.e.* somewhat fewer have been made so far, but there are still very many different multicomponent materials with different compositions but the same compound structure.[3,16] This includes intermetallic compounds such as the multicomponent monoaluminides MAl that have a single-phase B2 CsCl-type ordered bcc structure with all the aluminium atoms on one sublattice and a mixture of different metallic atoms distributed randomly on the other sublattice; ionic compounds such as the multicomponent mono-oxides MO that have a single-phase rock-salt ordered simple-cubic structure with all the oxygen atoms on the anion sublattice and a mixture of different metallic cations distributed randomly or near-randomly on the cation sublattice; and covalent compounds such as the multicomponent

diborides MB_2 that have a single-phase C32 TiB_2-type hexagonal structure, with a mixture of different metallic atoms distributed randomly or near-randomly on the lattice, each covalently bonded by two boron atoms.[3,16] Table 2 lists some of the compounds that have been shown to extend over a range of different compositions in multicomponent phase space.

A sufficiently large number of Cantor alloys have been investigated to allow a rough estimate of the extent of the single-phase fcc Cantor-alloy phase field from the different compositions that have been found to adopt a single-phase random or near-random fcc solid-solution structure. The maximum solubilities that have been found for individual components in single-phase fcc Cantor alloys[3,16,24] are shown in Table 3 and Fig. 2. Similarly, a sufficiently large number of Senkov alloys have been investigated to allow a rough estimate of the extent of

Table 3 Maximum solute contents in multicomponent single-phase fcc Cantor alloys

Solute max. at%							
Au	Pd	Pt	Zn	Nb	V	Ti	Mo
20	20	20	20	20	20	20	10
Solute max. at%							
Cu	Al	Cr	Mn	Fe	Co	Ni	
100	8	25	50	50	50	100	

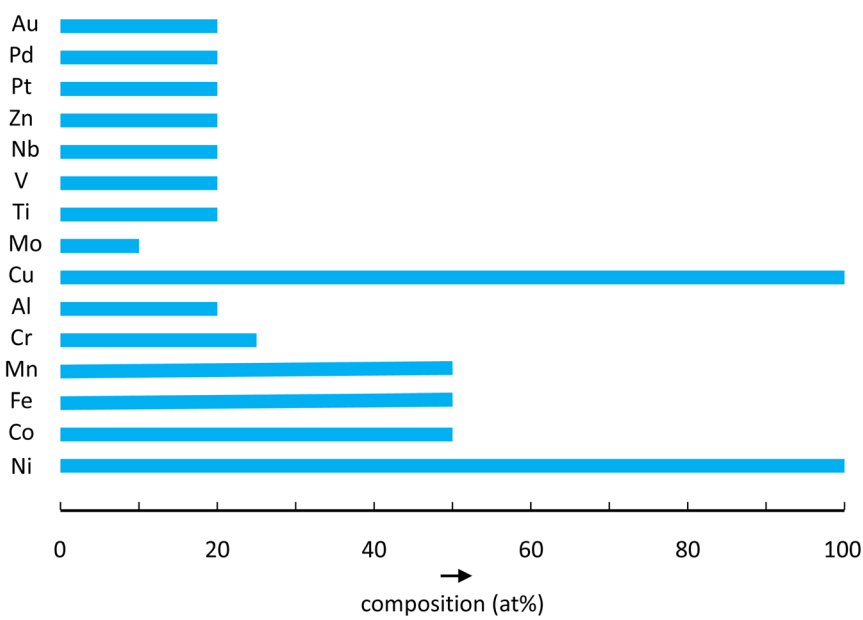

Fig. 2 Approximate maximum composition ranges for different components in single-phase fcc Cantor alloys.

Table 4 Maximum solute contents in multicomponent single-phase bcc Senkov alloys

Solute max. at%							
Re	Si	Al	Hf	Zr	Ti	W	Ta
8	2	30	30	30	30	100	100

Solute max. at%			
Mo	Nb	Cr	V
100	100	100	100

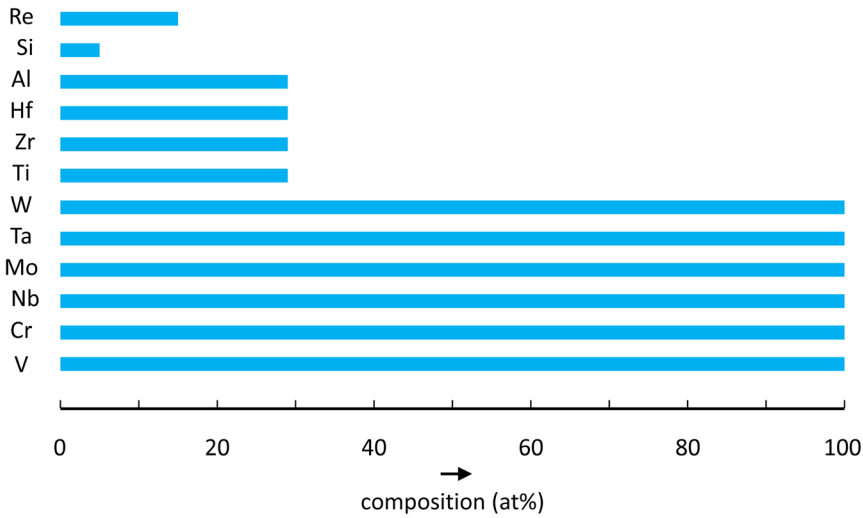

Fig. 3 Approximate maximum composition ranges for different components in single-phase bcc Senkov alloys.

the single-phase bcc Senkov-alloy phase field from the different compositions that have been found to adopt a single-phase random or near-random bcc solid-solution structure. The maximum solubilities that have been found for individual components in single-phase bcc Senkov alloys[3,16,26,27] are shown in Table 4 and Fig. 3. Solubility levels of any particular component vary, of course, with temperature, material composition and manufacturing method. Maximum solubilities such as those shown in Tables 3 and 4 are, therefore, almost certainly underestimates, since only a limited number of temperatures, material compositions and manufacturing methods have been investigated to date. Nevertheless, as can be seen in Tables 3 and 4, the multicomponent single-phase fcc Cantor and bcc Senkov alloy fields are both very large and complex in shape, each containing enormous numbers of different material compositions. It is likely that this is also the case for many other single-phase fields such as hcp, B2 monoaluminides, rock-salt mono-oxides, C32 diborides, and other phases[3,16] such as those listed in Table 2. These single-phase fields are separated in multicomponent phase space

by multiple-phase fields,[3,16] and it is almost certain that these also extend over wide ranges of different compositions. There is clearly a major experimental job to be done in mapping out the size and shape of all the different single-phase and multiple-phase fields in multicomponent phase space.

5. Are multicomponent materials difficult to manufacture?

In the 1970s, 1980s and 1990s, when Jien-Wei Yeh and I were working with our colleagues to study the first multicomponent high-entropy materials, it was widely believed that alloying with too much or too many alloying additions was undesirable and a bad idea, which is at least part of the reason why we were not encouraged to undertake our initial studies. It's not entirely clear why this was such a strong and widespread belief, though we can understand in general terms why it had developed. Historically, alloying was invented to improve the properties of particular materials. Thus, tin is added to copper in bronze to make it strong as well as formable;[28] carbon is added to iron in steels for a similar reason;[29] soda (sodium oxide) is added to silica (silicon oxide) in window glass to lower its melting point and make it easier to manufacture;[30] and phosphorus is added to silicon in semiconductors to increase the number of free electrons and enhance its electrical conductivity.[31] Adding too much of an alloying addition however, or adding too many alloying elements often makes a material difficult to manufacture, because of the formation of large quantities of brittle chemical compounds. Too much copper stannide Cu_6Sn_5, or cementite Fe_3C, or the formation of mullite $3Al_2O_3 \cdot 2SiO_2$ or silicon phosphide SiP, make bronze, steel, glass and silicon semiconductors respectively difficult or impossible to manufacture.[28–31] There are many other examples. It is well known, for instance, that the pick up of iron impurities in aluminium alloys needs to be kept lower than a fraction of a percent to prevent the embrittling effect of iron aluminide compounds,[32] and sulphur impurities in steels need to be kept to similarly low levels to prevent the embrittling formation of iron sulphides.[29] Essentially, a very strong taboo has developed over many years against making materials by using excessive alloying.

When alloying additions are increased beyond fairly low levels, the resulting materials often become, as just explained, relatively difficult to process, because of the formation of larger and larger quantities of brittle compounds. This seems to have led, as also just explained, to a strong and widespread tendency to avoid adding too much or too many alloying additions. We have now, however, studied enough multicomponent materials to know that this effect is not always maintained and indeed can often be reversed when we continue to add increasingly higher numbers and higher concentrations of alloying elements.[3,16] When enough alloying additions are made in sufficiently high concentrations, the tendency to form compounds is often, though not always, suppressed, leading instead to the formation in many cases of single-phase random solid-solution phases.[3,16] To summarise: in a large number of multicomponent materials, compound formation is suppressed, leading to a single-phase random solid-solution phase that is often easy to process; in a large number of other multicomponent materials,

however, compound formation is not suppressed, leading to the formation of a mixture of multiple compound phases, which is often not easy to process.

6. Why is compound formation often suppressed in multicomponent materials?

In a multicomponent material, the molar Gibbs free energy of the material G at any temperature T is given by:[33–35]

$$G = \sum_i x_i \mu_i^{ss} = \sum_i x_i \mu_i + \Delta G_{mix} = \sum_i x_i \mu_i + \Delta H_{mix} - T\Delta S_{mix}$$

where x_i is the molar fraction of the i'th component, μ_i and μ_i^{ss} are, respectively, the chemical potential (or molar free energy) of the i'th component before and after mixing to form the solution, and ΔG_{mix} $(= \Delta H_{mix} - T\Delta S_{mix})$, ΔH_{mix} and ΔS_{mix} are, respectively, the free energy of mixing, the heat (or enthalpy) of mixing and the entropy of mixing. The first term on the right hand side is the free energy of the unmixed components, and the last two terms are the free energy change caused by mixing them to form the final material. The heat of mixing ΔH_{mix} depends on the set of pairwise, three-way, four-way, *etc.*, interaction energies ω_{ij}, ψ_{ijk}, χ_{ijkl}, *etc.* (essentially the chemical bonding energies) between the different atoms in the material, *i.e.* $\Delta H_{mix} = f(\omega_{ij}, \psi_{ijk}, \chi_{ijkl}\ldots)$. The entropy of mixing ΔS_{mix} is the sum of two terms $\Delta S_{mix} = \Delta S_{mix}^{c} + \Delta S_{mix}^{xs}$, where ΔS_{mix}^{c} is the configurational entropy of mixing and ΔS_{mix}^{xs} is the excess entropy of mixing. The configurational entropy of mixing ΔS_{mix}^{c} comes mainly from the random mixing of different atoms in any solid-solution phases in the material, with a maximum value when the material forms a single-phase solid solution of $\Delta S_{mix}^{c} = -R\sum_i x_i \ln x_i$, where R is the gas constant, and a minimum value when the material forms a mixture of pure components and stoichiometric fixed-composition compounds of $\Delta S_{mix}^{c} = 0$.‡‡ The excess entropy of mixing ΔS_{mix}^{xs} comes from any other changes in disorder in the material and, like the heat of mixing, also depends on the set of pairwise, three-way, four-way, *etc.* interaction energies between the different atoms in the material, *i.e.* $\Delta S_{mix}^{xs} = f'(\omega_{ij}, \psi_{ijk}, \chi_{ijkl}\ldots)$, where f and f' are different functions. Overall, the Gibbs free energy is given, therefore, by:[33–35]

$$G = \sum_i x_i \mu_i^{ss} = \sum_i x_i \mu_i + \Delta G_{mix}$$
$$= \sum_i x_i \mu_i + \Delta H_{mix}(\omega_{ij}, \psi_{ijk}, \chi_{ijkl}\ldots) + RT\sum_i x_i \ln x_i - T\Delta S_{mix}^{xs}(\omega_{ij}, \psi_{ijk}, \chi_{ijkl}\ldots)$$

The first term on the right hand side is the free energy of the unmixed components and is independent of the final structure of the material; the sum of

‡‡ In this paper, the configurational entropy of mixing ΔS_{mix}^{c} is (for convenience, though somewhat unconventionally) taken to be determined by (only) the configurational entropy of mixing different atoms in solid-solution phases in the material; and other contributions to the configurational entropy of mixing, such as the entropy of distributing defects throughout the material (again for convenience, though somewhat unconventionally) are absorbed into the excess entropy of mixing ΔS_{mix}^{xs} alongside other contributions to the excess entropy of mixing, such as, for instance, changes in disorder arising from changes in the vibrational, electronic or magnetic states of the atoms in the material.

Table 5 Ideal entropy and Gibbs free energy of mixing $\Delta S_{mix} = -R \ln(1/c)$ and $\Delta G_{mix} = RT \ln(1/c)$ *versus* number of components c in an equiatomic multicomponent material (taking $R = 8.3145$ J K^{-1} mol^{-1})

Number of components c	$\ln(1/c)$	Ideal entropy of mixing ΔS_{mix} (J K^{-1} mol^{-1})	Ideal free energy of mixing ΔG_{mix} at 1000 K (kJ mol^{-1})
2	−0.69	5.76	−5.76
3	−1.10	9.13	−9.13
4	−1.39	11.53	−11.53
5	−1.61	13.38	−13.38
6	−1.79	14.90	−14.90
7	−1.95	16.18	−16.18
8	−2.08	17.29	−17.29
9	−2.20	18.29	−18.29
10	−2.30	19.12	−19.12
20	−3.00	24.91	−24.91
30	−3.40	28.28	−28.28
40	−3.69	30.67	−30.67
50	−3.91	32.53	−32.53

the last three terms adds up to the free energy of mixing, all of which are dependent on the final structure of the material. When a given set of components are mixed together to form a material, it can adopt a variety of different structures, and the final structure is the one with the lowest free energy G, which is the same, therefore, as the one with the lowest free energy of mixing ΔG_{mix}.[33–35]

The heat of mixing ΔH_{mix} usually favours compound formation, since it is determined by the interaction energies and the resulting chemical bonding between the different atoms in the material; on the other hand, the entropy of mixing ΔS_{mix} usually favours solid-solution formation, since its configurational component is determined by the disorder of mixing the different atoms closely together in the material. As mentioned in the introduction, most of our conventional materials have almost all been made from one, or sometimes two, main components, with relatively few alloying elements added in relatively dilute amounts. In conventional materials, therefore, the free energy of mixing ΔG_{mix} and the overall free energy G of the various possible material structures are usually dominated by the heat of mixing ΔH_{mix}. This means that compounds are formed readily when the interaction energies are positive (*i.e.* attractive, so that chemical bonds can form between the different atoms), so that compound formation increases with increasing number and concentration of the alloying elements, and the entropy of mixing ΔS_{mix} is relatively small, so that random or near-random solid solutions are only favourable at high temperatures.

The situation is different, however, in multicomponent materials, because the entropy of mixing can be much higher.[3,4,11,16] The maximum configurational entropy of mixing in any given alloy system is at the equiatomic composition, *i.e.* $\Delta S^{c}_{mix} = -R\sum_i x_i \ln x_i = -R \ln(1/c)$, where c is the number of components, and all x_i values are the same ($x_i = 0.5$ in a binary alloy, 0.33 in a ternary alloy, 0.25 in

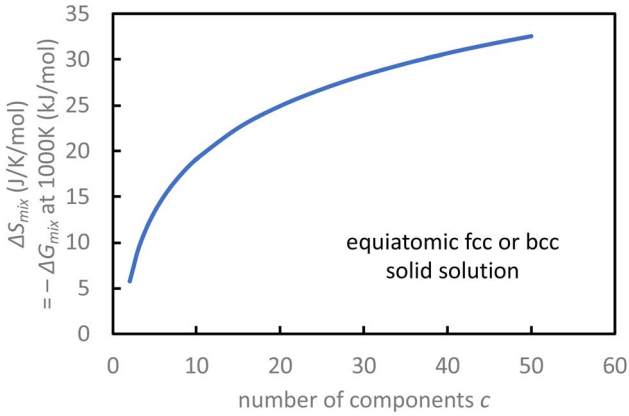

Fig. 4 Ideal entropy of mixing ΔS_{mix} and ideal free energy of mixing ΔG_{mix} at 1000 K for an equiatomic multicomponent material (such as the original Cantor alloy CrMnFeCoNi and Senkov alloy VNbTaMoW) *versus* the number of components c.

a quaternary alloy, *etc.*). Table 5 shows the resulting maximum ideal§§ entropy of mixing $\Delta S_{\text{mix}} = \Delta S^{\text{c}}_{\text{mix}} = -R\ln(1/c)$ and the corresponding ideal free energy of mixing $\Delta G_{\text{mix}} = -T\Delta S^{\text{c}}_{\text{mix}} = RT\ln(1/c)$ at 1000 K in such an equiatomic multicomponent material for different numbers of components ranging from $c = 2$ to 50. The same results are shown graphically in Fig. 4. The entropy of mixing in J K^{-1} mol^{-1} and the free energy of mixing at 1000 K (1273 °C) in kJ mol^{-1} are numerically equal and opposite, the first positive and the second negative. Differentiating:

$$\frac{\mathrm{d}\Delta G_{\text{mix}}}{\mathrm{d}c} = -T\frac{\mathrm{d}\Delta S^{\text{c}}_{\text{mix}}}{\mathrm{d}c} = -\frac{RT}{c} \to 0 \quad \text{as} \quad c \to \infty$$

so the ideal entropy of mixing increases monotonically and the ideal free energy of mixing decreases monotonically with increasing number of components c, but the rate at which the entropy of mixing increases and the rate at which the free energy of mixing decreases both slow down as the number of components rises.

An entropy of mixing below (approximately) the gas constant R, *i.e.* $\Delta S_{\text{mix}} \lesssim 8.3$ J K^{-1} mol^{-1} or $c \lesssim 3$, is lower than most of the interaction energies between the different atoms in a material, and is not, therefore, large enough to suppress compound formation in most materials;[3,16] on the other hand, an entropy of mixing above (approximately) the gas constant R, *i.e.* $\Delta S_{\text{mix}} \gtrsim 8.3$ J K^{-1} mol^{-1} or $c \gtrsim 3$, is higher than some or all of the interaction energies between the different atoms in a material, and is becoming high enough, therefore, to suppress compound formation in an increasing number of materials as the number of components increases.[3,16] Overall, therefore, compound formation is favoured when there are only low concentrations of a few alloying elements, since the

§§ In an ideal material, there are no chemical interactions between the different atoms in the material, the heat of mixing ΔH_{mix} and excess entropy of mixing $\Delta S^{\text{xs}}_{\text{mix}}$ are both, therefore, equal to zero, and the ideal free energy of mixing is determined by the configurational entropy of mixing $\Delta G_{\text{mix}} = -RT\Delta S^{\text{c}}_{\text{mix}} = RT\ln(1/c)$ for an equiatomic material.

configurational entropy of mixing is too low to outweigh chemical bonding effects, but compound formation becomes increasingly disfavoured when there are high concentrations (*e.g.* at equiatomic compositions) of many alloying elements (*i.e.* $c \gtrsim 3$), since the configurational entropy is then becoming high enough to outweigh chemical bonding effects. This explains why multicomponent materials were avoided for many years, when relatively small increases in alloying numbers and concentrations led to excessive compound formation, and the materials were found to be difficult to manufacture. It also explains our recent and, at first, surprising but now well-established discovery of large single-phase solid-solution regions in multicomponent phase space for equiatomic (and near-equiatomic or, at least, highly concentrated) compositions with five or more components, as discussed in previous sections.

It is worth pointing out, however, that an entropy of mixing even as high as (approximately) three or four times the gas constant R, *i.e.* $\Delta S_{\mathrm{mix}} \gtrsim 25$–$35\ \mathrm{J\ K^{-1}\ mol^{-1}}$ or $c \gtrsim 20$, is not larger than the interaction energies between the atoms in a material when they are very different chemically, and the resulting chemical bonds between them are very strong.[36] It seems likely, therefore, that when the number of components is increased to more than (say) ten or twelve, *i.e.* $c \gtrsim 10$–12, the inevitable chemical differences and interaction energies between an increasingly wide range of different elements become too large, and compound formation again takes over. This has not yet been fully established, but it would explain why extensive solid-solution formation has been discovered for multicomponent materials when most of the components are relatively similar chemically, *e.g.* for single-phase fcc Cantor alloys containing predominantly late transition elements, or single-phase bcc Senkov alloys containing predominantly early transition elements.

7. How stable are multicomponent high-entropy materials?

As discussed in previous sections, one of the first major discoveries in multicomponent materials was the single-phase fcc structure of the original Cantor alloy CrMnFeCoNi.[4] This was a big surprise because it was thought that increasing alloying content would lead to excessive compound formation, making multicomponent materials impossible to manufacture. It was particularly surprising for this material, given that only one of the five components (Ni) has an fcc structure at room temperature, and that materials made of binary and ternary mixtures of the five different components are well known to form stable compounds (such as $CrMn_3$, CrFe, Cr_3Co_2, MnNi, $FeNi_3$ and FeCo).[4] As also discussed in previous sections, it was further discovered and is now well established that multicomponent single-phase fcc Cantor alloys are formed over a wide range of compositions, including as many as eight or ten or even more mostly late transition-metal components;[3,16,24] that similar behaviour is exhibited by single-phase bcc Senkov alloys, also including as many as eight or ten or even more mostly early transition-metal components;[3,16,26,27] and that similar behaviour is also exhibited in many multicomponent compound structures, including intermetallic, ionic and covalently bonded materials.[3,16] As also discussed in previous sections, we now know that this behaviour is because of the increasing configurational entropy in multicomponent materials with more than three or four

components, which can suppress compound formation as long as the multiple components are not too different chemically, so that their interaction and chemical-bonding energies are not too large.[3,11,16,36]

Many experimenters have manufactured the original Cantor alloy *via* many different methods and subjected it to a wide range of different mechanical and thermal treatments, in almost all cases finding it to have a single-phase fcc structure that was easy to manufacture and apparently highly stable.[3,16] There was a certain degree of schadenfreude, therefore, when it was first reported that small compound precipitates had been found after extended heat treatment of the original Cantor alloy.[37,38] However, decomposition of the solid solution *via* precipitation only took place after annealing for several years in a fairly narrow temperature range, and it should not really have been a surprise. It is quite obvious from the functional form of the free energy of a material that entropy effects must become vanishingly small as the temperature decreases (since the second term in $\Delta G_{\mathrm{mix}} = \Delta H_{\mathrm{mix}} - T\Delta S_{\mathrm{mix}}$ goes to zero). In fact the third law of thermodynamics says that all materials at absolute zero must form mixtures of perfect single crystals, *i.e.* mixtures of pure components and fixed-composition compounds. It is similarly quite obvious from the functional form of the free energy of a material that entropy effects must become completely dominant as the temperature increases (since the second term in $\Delta G_{\mathrm{mix}} = \Delta H_{\mathrm{mix}} - T\Delta S_{\mathrm{mix}}$ increases without bound). In fact, all materials must become fully mixed atomically at sufficiently high temperatures. All materials will, therefore, in principle separate and decompose from an atomically mixed solution into a mixture of pure components and fixed-composition compounds (sometimes, though not always by precipitation) as they are cooled from high temperature. The only question is how strong are the compound-forming chemical interaction energies between the different atoms in the material relative to the solution-forming configurational entropy of mixing them intimately together; how high, therefore, is the critical temperature above which the equilibrium structure of a material is a solution and below which its equilibrium structure is a mixture of separated phases? In many cases, the chemical interaction energies are strong, much greater than the configurational entropy, and the critical temperature is well above the melting point, so that no solid-solution phase can form, but a liquid solution is often formed at high temperatures above the melting point. In many other cases, the chemical interaction energies are less strong, *i.e.* of a similar size to or somewhat lower than the configurational entropy, and the critical temperature is then below the melting point, so that a solid solution is formed at high temperatures, but it separates into a mixture of pure components and compounds as the material is cooled down to room temperature.[3,16] In some other cases, however, the chemical interaction energies are so much lower than the configurational entropy that the critical temperature is far below the melting point, approaching or even below room temperature, and a solid-solution again forms at high temperatures, but it does not separate into a mixture of pure components and compounds because the critical temperature is too low for significant atomic diffusion to take place.[3,16] To put it another way, solutions are always thermodynamically stable at high temperatures; they sometimes decompose (by precipitation) during cooling to room temperature; but they also sometimes fail to decompose during cooling to room temperature and are instead kinetically stabilised at low temperatures. Whether decomposition takes place depends on the relative strength of the

chemical-bonding interaction energies and the configurational entropy of the solution, with the balance between them determining the critical temperature at which decomposition takes place.

We now know[37,38] that the original Cantor alloy CrMnFeCoNi has a critical temperature approximately equal to 800 °C, so that a single-phase fcc solid solution is thermodynamically stable at high temperatures $T \gtrsim 800$ °C; precipitation takes place very slowly during annealing for many years in a band of intermediate temperatures 450 °C $\lesssim T \lesssim$ 750 °C; and a single-phase fcc solid solution is kinetically stable at low temperatures $T \lesssim 400$ °C. Similar behaviour is expected for single-phase solid solutions in many different multicomponent materials, *i.e.* thermodynamic stability at high temperatures, kinetic stability at low temperatures, and (sometimes) decomposition into multiple phases at intermediate temperatures after very extended heat treatment.

8. Are high-entropy materials ideal solid solutions?

Multicomponent phase space is very large and contains many materials. The answer to many general questions about the materials in multicomponent phase space is, therefore, very often both yes and no. Thus, as discussed previously, many multicomponent materials are found to be high-entropy single-phase solid solutions, but on the other hand, many other multicomponent materials are found not to be high-entropy materials and instead to be multiphase materials. Similarly, many high-entropy materials are ideal or near-ideal (regular¶¶) random solid solutions with no detectable short-range order, but many other high-entropy materials are found to be non-ideal and non-regular solid solutions, with a noticeable short-range order.[3,16]

In an ideal or regular solid solution, the atoms are distributed at random on the crystal lattice, and the probability of finding an atom of one of the components at any particular lattice point is proportional to its molar fraction, independent of the surrounding environment, *i.e.* independent of its neighbouring atoms. In a non-regular solid solution, however, the probability of finding an atom of one of the components at any particular lattice point is not proportional to its molar fraction, and is not independent of its neighbouring atoms. To be more specific, the probability $p_{ij}^{\,n}$ of two atoms of components i and j being nth near neighbours is given by $p_{ij}^{\,n} = x_i x_j$ in an ideal or regular solid solution, and by $p_{ij}^{\,n} \neq x_i x_j$ in a non-regular solid solution, where x_i and x_j are the molar fractions of the i'th and j'th components, respectively.[39] Non-ideal and non-regular solid solutions exhibit short-range order, with an increased probability for either association or disassociation of any particular pair of component atom types i and j in any particular near-neighbour shell n, driven by the non-zero pairwise, three-

¶¶ An ideal solution is one in which the interaction energies between the different atoms in the material are zero, so the heat of mixing is zero and the atoms are completely randomly mixed; a near-ideal or regular solution is one in which the interaction energies between the different atoms in the material are not zero but are very small, so the heat of mixing is not zero but the atoms are still completely randomly mixed; a non-regular solution is one in which the interaction energies between the different atoms in the material are not zero and are not small, so the heat of mixing is not zero, the atoms are not completely randomly mixed, and the solution exhibits short-range order.

way, four-way, *etc.* interaction energies between the different atoms ω_{ij}, ψ_{ijk}, χ_{ijkl}, *etc.* that contribute to the heat of mixing and the corresponding deviation from a random distribution of atoms. Instead of using the probabilities p_{ij}^{n} themselves, short-range order effects are usually quantified[39] by the Warren–Cowley short-range order (SRO) parameters $\alpha_{ij}^{n} = 1 - (p_{ij}^{n}/x_i x_j)$. In an ideal or regular solution, the SRO parameters α_{ij}^{n} are all zero, and in a non-regular solution they are either positive or negative for, respectively, the disassociation or association of atoms of components i and j as nth near neighbours.

Many multicomponent high-entropy materials are ideal or very near-ideal single-phase solid solutions. The original Cantor alloy is often found to be ideal or very close to ideal, with as far as we can tell a completely random distribution of the five component atoms (Cr, Mn, Fe, Co and Ni) and with no detectable short-range order. This can be seen in the atom probe (AP) measurements in Fig. 5, showing an even distribution of each of the five

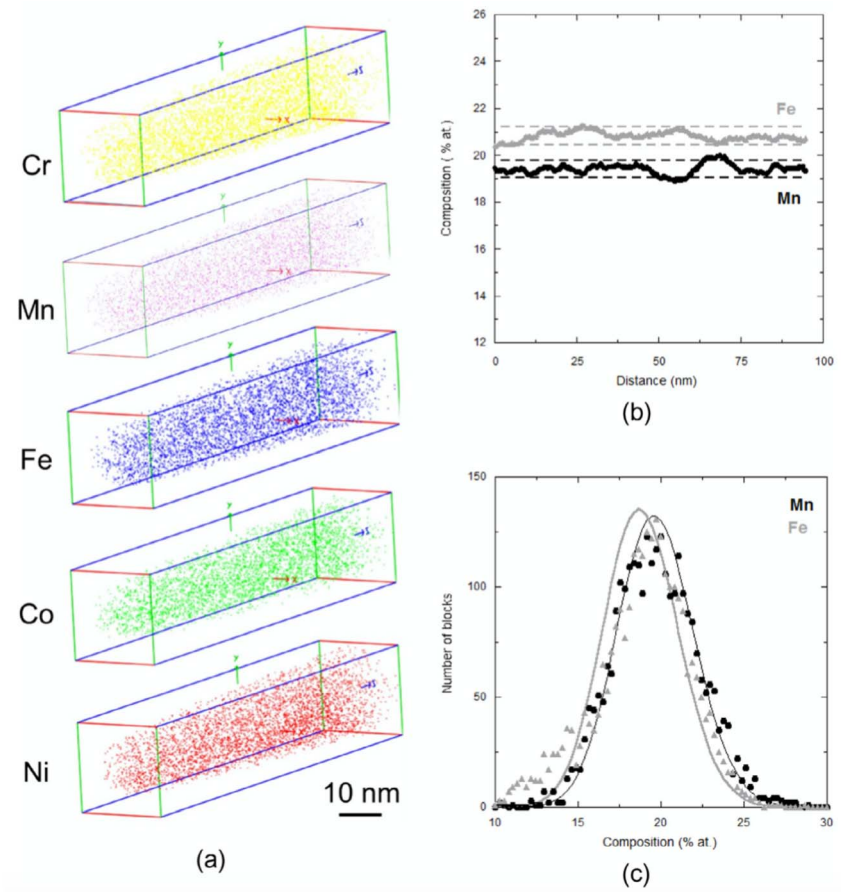

Fig. 5 Atom probe measurements from a recrystallised specimen of the single-phase fcc Cantor alloy CrMnFeCoNi, showing a random atomic-scale distribution of all five components: (a) composition maps (each point is a single atom); (b) composition profiles for Mn and Fe; and (c) random Gaussian composition distributions for Mn and Fe (after Laurent-Brocq *et al.*[40]). Reproduced with permission from Elsevier from ref. 40.

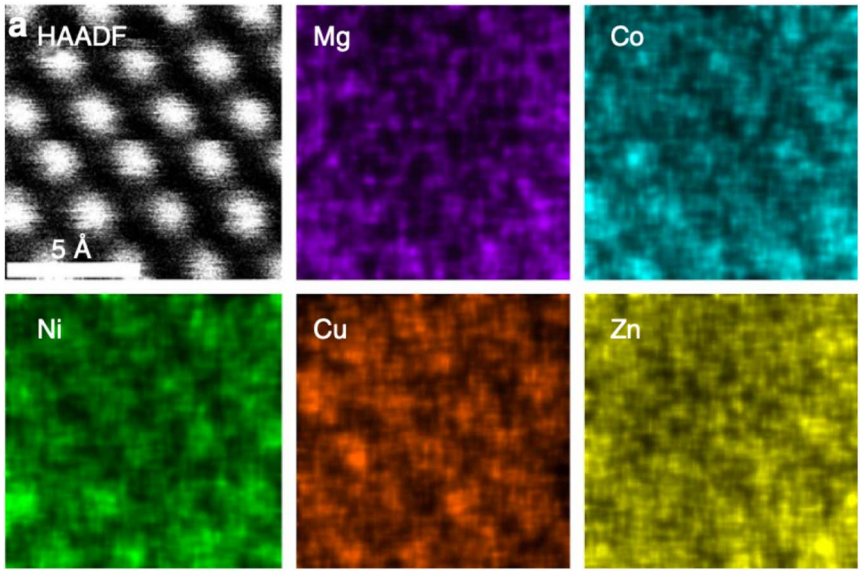

Fig. 6 HAADF-STEM atomic image of the single-phase multicomponent oxide (MgCoNiCuZn)O, and corresponding atomic-scale energy-dispersive X-ray (EDX) maps for each of the five cations, showing even intensities from a near-random distribution of cations on the cation sub-lattice (after Rost *et al.*[41]).

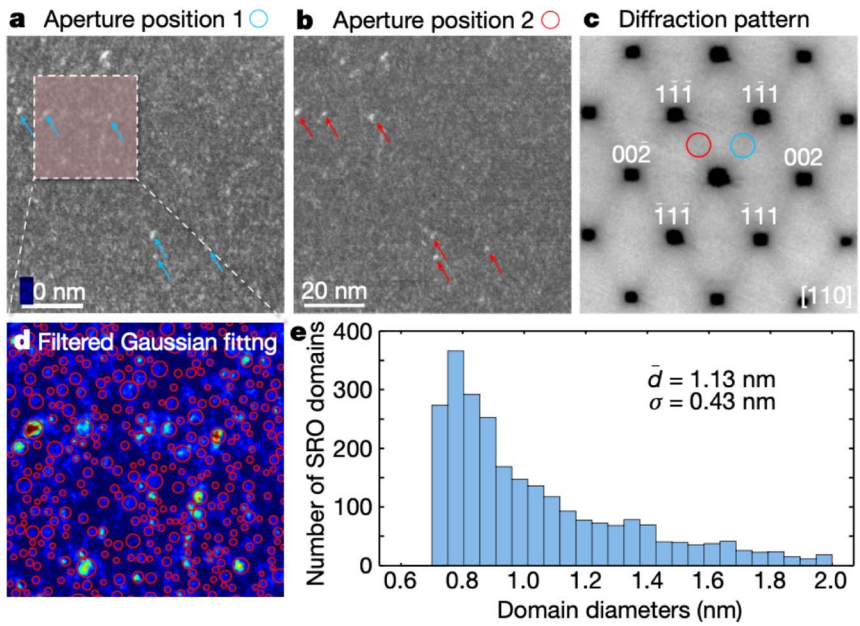

Fig. 7 HRTEM of modified Cantor alloy CrCoNi after homogenisation: (a) and (b) filtered dark-field images using blue and red selected-area diffraction apertures, respectively; (c) diffraction pattern; (d) filtered Gaussian fitting showing nm-sized domains; and (e) domain size distribution (after Zhang *et al.*[42]). Reproduced with permission from Springer Nature from ref. 42.

component atoms in CrMnFeCoNi, with statistical analysis confirming a random pattern in each case.[40] Similar results have also been found in other multicomponent materials, such as the single-phase rock-salt-structured mixed Rost oxide (MgCoNiCuZn)O. This can be seen[41] in the high-angle annular dark-field (HAADF) image and associated high-resolution energy-dispersive X-ray (EDX) maps in Fig. 6, again showing an even distribution of each of the five cations (Mg, Co, Ni, Cu and Zn) in (MgCoNiCuZn)O. There are also many multicomponent high-entropy materials that are non-ideal single-phase solid solutions. The simpler equiatomic three-component single-phase fcc modified Cantor alloy CrCoNi is considerably less homogeneous than the original five-component Cantor alloy, and contains small ~1 nm-sized domains of short-range ordering with enhanced Cr–Co and Cr–Ni and depleted Cr–Cr pairs in the 1st near-neighbour shell, *i.e.* with negative α^1_{CrCo} and α^1_{CrNi}, and positive α^1_{CrCr}, as shown in the high-resolution transmission electron microscope (HRTEM) images[42] in Fig. 7. Another example can be seen in the atom-probe (AP) measurements[43] in Fig. 8 from a quaternary single-phase bcc modified Senkov alloy ZrNbTaHf, showing short-range clustering of Zr and Hf atoms, *i.e.* negative α^1_{ZrZr}, α^1_{HfHf} and α^1_{ZrHf} and corresponding positive α^1_{ZrNb}, α^1_{ZrTa}, α^1_{NbHf} and α^1_{TaHf}, that builds up progressively with annealing time at 1800 °C (2073 K), beginning with small nm-sized regions of SRO and finally forming a 3-D phase-separated network on a scale of ~10 nm.

As mentioned in the last section, all high-entropy solid solutions must in principle decompose to form a multiphase structure on cooling to room

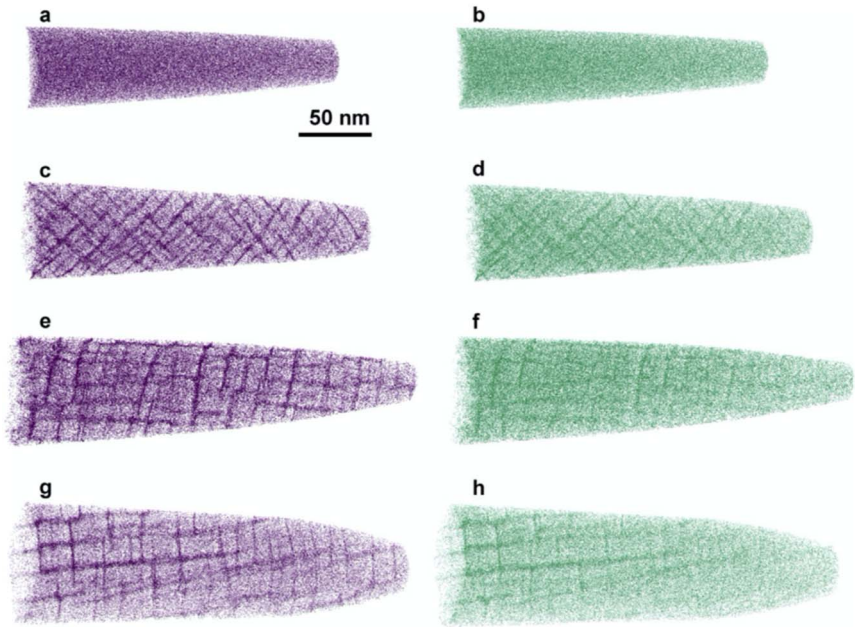

Fig. 8 AP composition profiles for Zr (purple) and Hf (green) from modified Senkov alloy ZrNbTaW: (a) and (b) as-cast, and after annealing at 1800 °C for (c) and (d) 6 hours, (e) and (f) 1 day, and (g) and (h) 4 days (after Maiti and Steurer[43]). Reproduced with permission from Elsevier from ref. 43.

temperature, driven by the interaction energies between the different atoms in the material. But many will not do so, when the interaction energies are relatively weak and the configurational entropy is relatively high, so that the critical temperature for decomposition is too low for significant atomic diffusion to take place.[3,16,36] All high-entropy solid solutions must also in principle exhibit short-range ordering, typically at temperatures in the vicinity of the critical temperature for decomposition (with stable short-range order forming just above the critical temperature, and transitory short-range order forming as a precursor to precipitation just below the critical temperature), again driven by the interaction energies between the different atoms in the material.[3,16,36] But similarly many will not do so, again when the critical temperature is too low for significant atomic diffusion to take place.[3,16,36] Some multicomponent materials, like the original five-component Cantor alloy CrMnFeCoNo, have a low critical decomposition temperature and are, therefore, stable as a high-entropy near-ideal random solid solution, rarely exhibiting short-range order and decomposing only with difficulty after very prolonged heat treatment.[37,38,40] Other multicomponent materials, however, like the three-component modified Cantor alloy CrCoNi or the four-component modified Senkov alloy ZrNbTaHf, have a high critical decomposition temperature and are, therefore, relatively unstable, frequently exhibiting significant short-range order and decomposing easily and rapidly during cooling to room temperature or after relatively short subsequent heat treatment.[42,43]

9. What is the local atomic structure in high-entropy materials?

It is rather obvious that multicomponent single-phase materials such as, for instance, the original five-component fcc Cantor alloy CrMnFeCoNi or the original five-component bcc Senkov alloy VNbMoTaW, are different from corresponding single-component single-phase materials such as, for instance, pure fcc Cu or pure bcc Fe, because there are different atoms with different properties distributed in a random or near-random way across the different lattice points rather than the same atom with identical properties at every lattice point. But the variation in local structure and properties in multicomponent high-entropy single-phase solid-solution materials is much more extensive and complex, because the structure and properties at any lattice point depend not only on which atom is located there, but also on its interactions with its neighbouring atoms at nearby lattice points.[3,44] In other words, the variation in properties from lattice point to lattice point depends on the range of local atomic environments, *i.e.* on the range of different local atomic clusters of each atom and its surrounding near-neighbours.

Consider a general lattice with a single atom at each lattice point, and with n_1, n_2 and n_3 first, second and third near neighbours respectively. The cluster size of each atom together with its first near neighbours is $n_1 + 1$ atoms, increasing to $n_2 + n_1 + 1$ atoms and then to $n_3 + n_2 + n_1 + 1$ atoms including second and then third as well as first near neighbours. The number of different clusters N_1 of $n_1 + 1$ atoms, N_2 of $n_2 + n_1 + 1$ atoms, and N_3 of $n_3 + n_2 + n_1 + 1$ atoms in a multicomponent

Table 6 Number of different oriented and non-oriented local atomic clusters N_1, N_2 and N_3 out to first, second and third near neighbours, respectively, for a multicomponent single-phase fcc material with c components

Number of components c	Oriented clusters			Non-oriented clusters		
	1st	2nd	3rd	1st	2nd	3rd
3	1.6×10^{6}	1.2×10^{9}	3.3×10^{20}	6.4×10^{4}	4.8×10^{7}	1.3×10^{19}
4	6.7×10^{7}	2.7×10^{11}	7.7×10^{25}	2.7×10^{6}	1.1×10^{10}	3.1×10^{24}
5	1.2×10^{9}	1.9×10^{13}	1.1×10^{30}	4.8×10^{7}	7.6×10^{11}	4.4×10^{28}
6	1.3×10^{10}	6.1×10^{14}	2.9×10^{33}	5.2×10^{8}	2.4×10^{13}	1.2×10^{32}
8	5.5×10^{11}	1.4×10^{17}	6.8×10^{38}	2.2×10^{10}	6.0×10^{15}	2.7×10^{37}
10	10^{13}	10^{19}	10^{43}	4.0×10^{11}	4.0×10^{17}	4.0×10^{41}
20	8.2×10^{16}	5.2×10^{24}	8.8×10^{55}	3.3×10^{15}	2.1×10^{23}	3.5×10^{54}
50	1.2×10^{22}	1.9×10^{32}	1.1×10^{73}	4.8×10^{20}	7.6×10^{30}	4.4×10^{71}

equiatomic single-phase material with a random (ideal or regular) arrangement of c components is given[22] by the law of permutations with repetition:||||

$$N_1 = c^{n_1+1}$$

$$N_2 = c^{n_2+n_1+1}$$

$$N_3 = c^{n_3+n_2+n_1+1}$$

These are orientation-dependent cluster numbers (*i.e.* equivalent clusters with a different orientation are regarded as different), as is appropriate when we are dealing with properties that depend on orientation, such as dislocation slip, diffusion or magnetisation, when the material is responding to an oriented vector of applied stress, concentration gradient or magnetic field, respectively. If cluster orientation is not significant, however, the number of different clusters is smaller because of the number of self-similarity operations s associated with the crystal symmetry:[45,46]

$$N_1 = (c^{n_1+1})/s$$

$$N_2 = (c^{n_2+n_1+1})/s$$

$$N_3 = (c^{n_3+n_2+n_1+1})/s$$

with $s = 24$ for instance for a cubic crystal.[45,46] These are orientation-independent cluster numbers (*i.e.* equivalent clusters with a different orientation are regarded

|||| We want to calculate how many ways we can pick $n_1 + 1$ (or, including second or second and third near neighbours, $n_2 + n_1 + 1$ or $n_3 + n_2 + n_1 + 1$) atoms from a total of c components. Let the atomic sites in the cluster be labelled 1, 2, 3, *etc.* up to $n_1 + 1$ (or $n_2 + n_1 + 1$ or $n_3 + n_2 + n_1 + 1$). Different sets of the c components distributed across the different atomic sites are clearly different, but different arrangements of any given set of c components across the different atomic sites are also different. In other words, we need an ordered permutation rather than a non-ordered combination. And we need a permutation with repetition since each of the different component atoms can be picked more than once.[22]

as the same), as is appropriate when we are dealing with properties that are independent of orientation, such as density or bulk modulus.

Table 6 shows the numbers of oriented and non-oriented local atomic clusters N_1, N_2 and N_3 for multicomponent equiatomic single-phase fcc Cantor alloys with c components, taking for fcc $n_1 = 12$, $n_2 = 6$ and $n_3 = 24$, so the cluster sizes are 13, 19 and 43 atoms, respectively.[3,44] Table 7 shows equivalent numbers for multicomponent equiatomic single-phase bcc Senkov alloys, taking for bcc $n_1 = 8$, $n_2 = 6$ and $n_3 = 12$, so the cluster sizes are 9, 15 and 27 atoms, respectively.[3,44] The same results are shown graphically in Fig. 9 and 10 for fcc and bcc respectively. It is obvious from Tables 6 and 7 and Fig. 9 and 10 that the numbers of different local atomic clusters in multicomponent single-phase materials are very large indeed. Many but not all of the properties of a material are determined by interactions between first and second near-neighbour atoms, and many but not all are orientation-dependent, so we concentrate here on the number of oriented, first and second near-neighbour, local atomic clusters, which is just under twenty trillion (1.9×10^{13}) for the original single-phase fcc Cantor alloy CrMnFeCoNi and just over thirty billion ($3.1 \times$

Table 7 Number of different oriented and non-oriented local atomic clusters N_1, N_2 and N_3 out to first, second and third near neighbours, respectively, for a multicomponent single-phase bcc material with c components

Number of components c	Oriented clusters			Non-oriented clusters		
	1st	2nd	3rd	1st	2nd	3rd
3	2.0×10^4	1.4×10^7	7.6×10^{12}	8.0×10^2	5.6×10^5	3.0×10^{11}
4	2.6×10^5	1.1×10^9	1.8×10^{16}	1.0×10^4	4.4×10^7	7.2×10^{14}
5	2.0×10^6	3.1×10^{10}	7.5×10^{18}	8.0×10^4	1.2×10^9	3.0×10^{17}
6	1.0×10^7	4.7×10^{11}	1.0×10^{21}	4.0×10^5	1.9×10^{10}	4.0×10^{19}
8	1.3×10^8	3.5×10^{13}	2.4×10^{24}	5.2×10^6	1.4×10^{12}	9.6×10^{22}
10	10^9	10^{15}	10^{27}	4.2×10^7	4.2×10^{13}	4.2×10^{25}
20	5.1×10^{11}	3.3×10^{19}	1.3×10^{35}	2.0×10^{10}	1.3×10^{18}	5.2×10^{33}
50	2.0×10^{15}	3.1×10^{25}	7.5×10^{45}	8.0×10^{13}	1.2×10^{24}	3.0×10^{44}

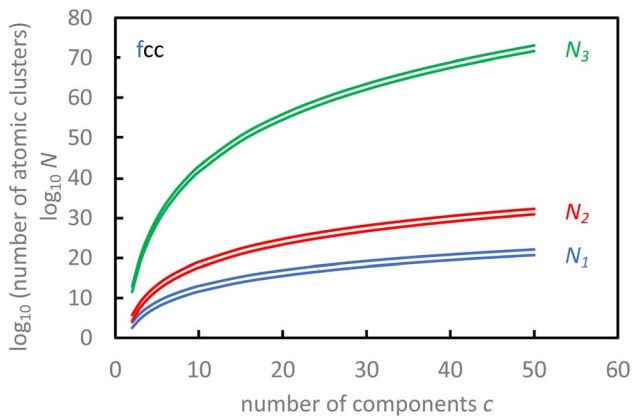

Fig. 9 Number of different oriented (upper lines) and non-oriented (lower lines) local atomic clusters out to first (N_1), second (N_2) and third (N_3) near neighbours for a multicomponent single-phase fcc material with c components.

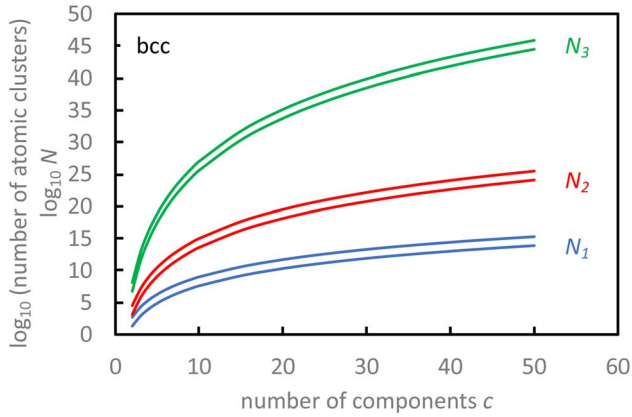

Fig. 10 Number of different oriented (upper lines) and non-oriented (lower lines) local atomic clusters out to first (N_1), second (N_2) and third (N_3) near neighbours for a multi-component single-phase bcc material with c components.

10^{10}) for the original single-phase bcc Senkov alloy, both with five components. With six components, the number of oriented, first and second near-neighbour, local atomic clusters increases to just over six hundred trillion (6.1×10^{14}) for fcc Cantor alloys and almost half a trillion (4.7×10^{11}) for bcc Senkov alloys; and with eight components, it is well over a quadrillion (1.4×10^{17}) for fcc Cantor alloys and over thirty trillion (3.5×10^{13}) for bcc Senkov alloys. The number of local atomic clusters is, of course, very much larger again if we include third near neighbours and/or increase the number of components to (say) ten or more, as shown in Tables 6 and 7 and Fig. 9 and 10. The number in all cases will be somewhat reduced, of course, if there is significant short-range ordering.

The number of local atomic clusters is very large indeed, and this has an important effect on the spatial consistency of the properties of multicomponent high-entropy single-phase solid solutions such as the fcc Cantor and bcc Senkov alloys.[3,44] Taking the cube root of the number of local atomic clusters gives the size of a piece of the material sufficiently large to include all possible local atomic configurations, *i.e.* a piece of the material big enough to average reasonably over all the different local atomic environments and, therefore, big enough to represent fully the material and its properties. The linear dimension of such a piece of material is $\sqrt[3]{1.9 \times 10^{13}} = 2.7 \times 10^4$ clusters or ~8 μm for oriented, first and second near-neighbour clusters in the original single-phase fcc Cantor alloy, and $\sqrt[3]{3.1 \times 10^{10}} = 3.1 \times 10^3$ clusters or ~1 μm in the original single-phase bcc Senkov alloy, in both cases taking the atomic separation and, therefore, the cluster size as ~0.3 nm. In other words, the properties of the original fcc Cantor and bcc Senkov alloys vary from grain to grain if their polycrystalline grain size is below ~8 μm or ~1 μm, respectively. To put it another way, the grain size needs to be above ~8 μm or ~1 μm, respectively, to have a material with consistent properties. And for equiatomic ten-component single-phase fcc Cantor or bcc Senkov alloys, the grain size needs to be above $\sqrt[3]{10^{19}} = 2.2 \times 10^6$ clusters ≈ 0.7 mm or $\sqrt[3]{10^{15}} = 10^5$ clusters ≈ 30 μm, respectively.

This is clearly a very different situation from that which is found in conventional materials consisting of either a single component or a single main

component with one or more dilute alloying additions. The extremely large number of different local atomic environments and atomic clusters in multi-component single-phase fcc and bcc solid solutions such as the Cantor and Senkov alloys (and in other crystal structures such as multicomponent intermetallic and ceramic compounds) plays, therefore, an important role in material properties that depend strongly on local atomic interactions, such as vacancy migration and diffusion, or dislocation slip and plastic flow.[3,44] The extremely large number of different local atomic environments and atomic clusters in these materials also makes it extremely difficult, in fact almost impossible, to determine their structure and properties with any degree of confidence by fundamental techniques such as *ab initio* molecular dynamics or quantum mechanical modelling that are limited to no more than a thousand or two atoms at best.

10. What is the local atomic strain in high-entropy materials?

Table 8 shows 12-coordinated metallic Goldschmidt atomic radii r for some of the components that have been used to manufacture multicomponent single-phase fcc Cantor alloys.[47] The maximum difference in atomic size amongst the five different components in the original Cantor alloy CrMnFeCoNi is $\Delta r = r_{Cr} - r_{Ni} =$ 3 pm, the corresponding maximum atomic misfit is $\delta_{max} = (r_{Cr} - r_{Ni})/r_{Ni} = 2.4\%$, and the root-mean-square (RMS) average atomic misfit is $\delta_{av} = \sqrt{\sum_i x_i\{(r_i - r_{av})/r_{av}\}^2} = 0.9\%$, where summation is over all the components $i = 1$ to n, $x_i = 0.2$ is the mole fraction of the i'th component, and $n = 5$ is the number of components. The values of Δr, δ_{max} and δ_{av} remain unchanged when Cu is included in a modified CrMnFeCoNiCu_x Cantor alloy, but they are somewhat larger when Al instead of Cu is included in a modified Al_xCrMnFeCoNi Cantor alloy: $\Delta r = 18$ pm, $\delta_{max} = 14.4$, and $\delta_{av} = 1.4\%$, for the maximum Al solubility with $x_{Al} = 8\%$ and $x_{i\neq Al} = 18.4\%$. We might expect, therefore, to find lattice distortions on a scale of somewhat under ~1 pm or 1% on average, rising to a maximum of ~3 pm or ~3% in the original Cantor alloy, and a bit higher in some of the modified Cantor alloys, such as those containing Al. These calculations are rather approximate since they ignore effects such as short-range order, non-ideality, relaxation, and electronic distortions. More detailed analyses have

Table 8 Goldschmidt atomic radii r for some of the components used to manufacture fcc Cantor alloys[47]

Component	Goldschmidt atomic radius r (pm)
Cr	128
Mn	127
Fe	126
Co	125
Ni	125
Al	143
Cu	128

Table 9 Experimental and calculated values for the maximum local atomic distortion Δr in the equiatomic fcc Cantor alloy CrMnFeCoNi, obtained *via* a variety of different methods[47–52]

	Method	Maximum local atomic distortion Δr (pm)
Calculations	Goldschmidt radii	3.0
	Ab initio	3.3–6.6
Experiments	Synchrotron XRD	4.8
	Neutron diffraction	2.0
	EXAFS	3.8

used measured lattice parameters, different definitions of atomic misfit and lattice distortion, and *ab initio* calculations, but all lead to similar predicted local lattice distortions[48–51] of $\Delta r \approx 3.3$–6.6 pm.

Lattice distortions have been measured in multicomponent solid solutions *via* synchrotron X-ray diffraction (XRD),[48] neutron diffraction (ND)[52] and extended X-ray absorption fine-structure (EXAFS) analysis.[49,53] The measurements are difficult because of the need to separate static displacements caused by lattice distortions, dynamic displacements caused by thermal vibrations, and bulk lattice strain. Sophisticated fitting software is used with high-quality diffraction data to separate out different effects within the measured broadening of diffraction peaks. Okamoto *et al.*[48] used single-crystal synchrotron X-ray diffractometry to measure atomic displacements in the original Cantor alloy of 4.8 and 7.7 ± 0.5 pm at 25 K and 300 K, respectively, indicating a static displacement (at 25 K) of $\Delta r \approx 4.8$ pm and a thermal displacement (at 300 K) of $7.7 - 4.8 = 2.9$ pm. Owen *et al.*[52] used neutron powder diffractometry to measure partial distribution functions in the original Cantor alloy, with different peak widths between the Cantor alloy and pure Ni corresponding to static distortions of $\Delta r \approx 2 \pm 0.5$ pm and the underlying peak width giving thermal distortions of $\sim 18 \pm 0.5$ pm. Oh *et al.*[49] used EXAFS spectra from the original Cantor alloy to obtain mean elemental distortions of +0.1%, +0.5%, −0.1%, −0.4% and −0.1% for Cr, Mn, Fe, Co and Ni respectively,*** correlating roughly with the Goldschmidt atomic radii in Table 8, and with maximum distortions up to ~3% of r_{av} (=126.2 pm), *i.e.* $\Delta r \approx 3.8$ pm.

Table 9 shows experimental and calculated results for local distortions Δr in the original fcc Cantor alloy CrMnFeCoNi. In conclusion, there are small but significant local lattice distortions that fluctuate randomly over large distances (because of the enormous number of different local atomic cluster configurations), with an average value of just under 1 pm (corresponding to just under ~1% strain), reaching a maximum value of ~2–6 pm (corresponding to ~2–6% strain). Similar measurements and calculations indicate, as expected, somewhat smaller lattice distortions in simpler fcc Cantor alloy compositions such as CrFeCoNi,[50,53–55] but somewhat larger lattice distortions in modified Cantor alloy compositions containing additional components such as VFeCoNi[56] and FeNiCoCrPd.[55]

Table 10 shows 12-coordinated metallic Goldschmidt atomic radii r for some of the components that have been used to manufacture multicomponent single-

*** Positive and negative values represent increased and decreased bond lengths respectively, corresponding to local atomic expansion and compression strains, respectively.

Table 10 Goldschmidt atomic radii r for components used to manufacture bcc Senkov alloys.[47]

Component	Goldschmidt atomic radius r (pm)
V	135
Nb	145
Mo	145
Ta	145
W	135
Al	143
Ti	140
Zr	155
Hf	155

phase bcc Senkov alloys.[47] The maximum difference in atomic size amongst the five different components in the original Senkov alloy VNbMoTaW is $\Delta r = r_{Nb} - r_V = 10$ pm, the corresponding maximum atomic misfit is $\delta_{max} = (r_{Nb} - r_V)/r_V = 7.4\%$, and the root-mean-square (RMS) average atomic misfit is $\delta_{av} = \sqrt{\sum_i x_i\{(r_i - r_{av})/r_{av}\}^2} = 3.5\%$. The values of Δr, δ_{max} and δ_{av} remain unchanged when either Al or Ti are included in modified Al_xVNbMoTaW or Ti$_x$VNbMoTaW Senkov alloys, respectively, but they are somewhat larger again when either Zr or Hf is included in modified VNbZr$_x$MoTaW or VNbMoHf$_x$TaW Senkov alloys, respectively, for an equiatomic six-component alloy with $x_i = 16.67\%$. We might expect, therefore, to find lattice distortions on a scale of ~4 pm or ~4% on average, rising to a maximum of ~7–10 pm or ~10% in the original Senkov alloy, and still higher in some of the modified Senkov alloys, such as those containing Zr or Hf. These calculations are again rather approximate since they ignore effects such as short-range order, non-ideality, relaxation, and electronic distortions. Other analyses of the lattice distortion have again used *ab initio* calculations, leading to similar predicted local lattice distortions of $\Delta r \approx$ 5–15 pm.[50]

Zou *et al.*[57] used single-crystal X-ray diffractometry to measure average atomic displacements in the original Senkov alloy, indicating static and dynamic lattice distortions of $\Delta r \approx 7.4$ and 6.1 ± 0.5 pm, respectively. Lattice distortions on a scale of tens of pm have also been observed by Zou *et al.*[57] in the same alloy *via* high-resolution transmission electron microscopy (HRTEM), with [100] zone axis images containing distorted {110} planes, as shown in Fig. 11. Guo *et al.*[58] used a combination of synchrotron X-ray diffractometry (XRD) and time-of-flight (TOF) neutron diffractometry to obtain radial distribution functions from a modified ternary Senkov alloy ZrNbHf, with an overlap of the first and second near-neighbour peaks corresponding to lattice distortions of ~9.5 pm, and similar combined XRD and ND results for a quaternary modified Senkov alloy ZrNbTaHf showed static and dynamic thermal distortions of 13.7 and 2.4 pm, respectively.[59]

Table 11 shows experimental and calculated results for maximum local distortions Δr in bcc Senkov alloys. In conclusion, there are again significant local lattice distortions in the bcc Senkov alloys, somewhat larger than those found in the fcc Cantor alloys, that again fluctuate randomly over large distances (because of the enormous number of different local atomic cluster configurations), with

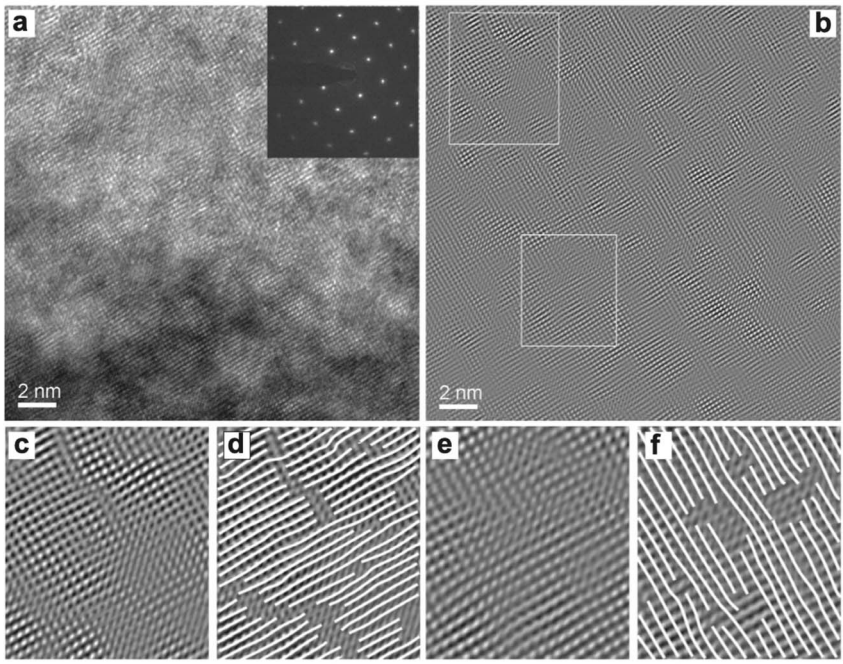

Fig. 11 HRTEM images of the equiatomic quaternary NbMoTaW bcc Senkov alloy: (a) bright-field (BF) image with [100] zone axis; (b) corresponding inverse fast-Fourier transform; (c) and (e) enlarged images of the boxes in (b); and (d) and (f) traces corresponding to (c) and (e) to show the lattice distortions (after Zou *et al.*[57]). Reproduced with permission from Elsevier from ref. 57.

average values of ~4 pm (corresponding to ~4% strain), reaching maximum values of ~5–20 pm (corresponding to >5% strain).

It is highly likely that similar substantial local atomic strains are to be found in all multicomponent high-entropy single-phase solid-solutions, extending over large distances, and influencing many of their properties.

Table 11 Experimental and calculated values for the maximum local atomic distortion Δr in the bcc Senkov alloys, obtained *via* a variety of different methods[47,50,56–59]

	Method	Alloy	Maximum local atomic distortion Δr (pm)
Calculations	Goldschmidt radii	VNbMoTaW AlVNbMoTaW TiVNbMoTaW	10.0
	Goldschmidt radii	VNbZrMoTaW VNbMoHfTaW	20.0
	Ab initio	TiVNb AlTiVNb TiZrNbTaHf	5–15
Experiments	XRD	NbMoTaW	4.8
	Synchrotron XRD & ND	ZrNbHf	9.5
	Synchrotron XRD & ND	ZrNbTaHf	13.7

11. What is the effect of varying local atomic strain?

11.1 Vacancies and diffusion

Atomic motion leads to the degradation of crystalline materials when they are exposed, for instance, to high temperatures, irradiation or a corrosive environment. And atomic motion usually takes place in crystalline materials *via* vacancy migration.[35,60,61] The probability of finding a vacancy at any lattice point p_v and the probability of vacancy motion (*i.e.* of an adjacent atom jumping into it) p_m are both given at any temperature T by Boltzmann's equation:[35,60,61]

$$p_v \propto \exp\left(-\frac{\Delta E_v}{kT}\right)$$

$$p_m \propto \exp\left(-\frac{\Delta E_m}{kT}\right)$$

where ΔE_v and ΔE_m are the vacancy formation and migration energies respectively and k is Boltzmann's constant. In a single-component pure material, ΔE_v and ΔE_m and, therefore, p_v and p_m are all independent of position because all the lattice sites are identical. Atomic motion takes place, therefore, *via* a random walk and obeys Fick's laws, with a diffusion coefficient D that depends on p_v and p_m:

$$D \propto p_v p_m = D_o \exp\left(-\frac{Q}{kT}\right)$$

where D_o and $Q = \Delta E_v + \Delta E_m$ are, respectively, the frequency factor and the activation energy for diffusion.[35,60,61]

Atomic motion in a concentrated multicomponent high-entropy solid solution, such as an fcc Cantor alloy or a bcc Senkov alloy, is more complex because of the wide variety of different local atomic structures and associated lattice distortions surrounding the vacancies, and a correspondingly wide range of different vacancy formation and migration energies ΔE_v and ΔE_m, depending upon where the vacancy is and what exactly are its surrounding atoms.[3,44] There is an enormous number of different local atomic clusters surrounding each individual type of atom in a multicomponent solid solution (as discussed previously and as shown in Tables 6 and 7 and Fig. 9 and 10): and there is a similarly enormous number of different local atomic clusters surrounding the vacancies in a multicomponent solid solution or, to put it in another way, there is an enormous number of different vacancy structures.[3,44]

There is little or no lattice distortion in a single-component pure material, and the variation of energy as an individual vacancy hops from one lattice site to another consists of a series of identical jumps, as shown schematically in Fig. 12, from identical wells at each of the lattice sites, all with the same well energy E_w, over identical saddle points midway between each of the lattice sites, all with the same saddle-point energy E_s. In a concentrated multicomponent high-entropy solid solution, however, the situation is very different, because of the large number of vacancy structures and associated local lattice distortions at different lattice points, the corresponding range of vacancy formation and migration

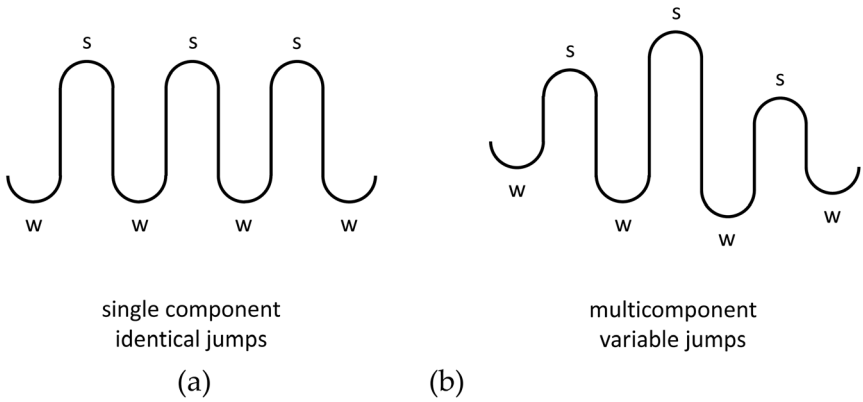

Fig. 12 Schematic variation of energy as a vacancy hops from lattice site to lattice site: (a) in a single-component material with all jumps identical; and (b) in a multicomponent material with variable jumps (s = saddle point energy; w = energy well).

energies ΔE_v and ΔE_m, and the corresponding spread of well and saddle-point energies E_w and E_s. The variation in energy of an individual vacancy as it hops from one lattice site to another consists instead, therefore, of a series of variable jumps, as also shown schematically in Fig. 12, from variable wells at the different lattice sites, all with different well energies E_w, over variable saddle points midway between each of the lattice sites, all with different saddle-point energies E_s.

The overall rate of atomic diffusion and, therefore, the diffusion coefficient in concentrated multicomponent high-entropy solid-solution materials is affected in a variety of ways[44,62] by the variation in vacancy formation and migration energies ΔE_v and ΔE_m, and the corresponding spread of well and saddle point energies E_w and E_s. High-energy barriers in some places make it particularly difficult for a vacancy to hop from one site to the next; low energy barriers in other places make it particularly easy for a vacancy to hop from one site to the next; and a vacancy can be trapped in some places, hopping backwards and forwards between adjacent or near-adjacent lattice points, or going round and round in circles. The overall impact of these different effects is, not surprisingly, quite complex, and strictly speaking, diffusion is no longer truly random spatially, since the lattice points are no longer all identical. We have not yet made much experimental or theoretical progress towards developing a detailed understanding of this complex range of different vacancy behaviours and the resulting overall rates of atomic diffusion. Thomas and Patala[62] calculated the expected spread of well and saddle-point energies E_w and E_s for vacancies hopping between adjacent lattice sites at 1000 °C in the original five-component single-phase fcc Cantor alloy CrMnFeCoNi, using a nudged elastic band (NEB) molecular dynamics (MD) method with a modified embedded atom method (MEAM) potential within the Sandia Labs LAMMPS software. The diffusion coefficient D was found to be fairly sensitive to the spread of energy values during the hopping process, varying between a half and five times a reference diffusion coefficient D^* in an equivalent material with the same barrier energy of 0.81 eV, but with constant well and saddle-point energies. The exact results obtained *via* these calculations should be treated with considerable caution (as with other modelling results), since they

average over only about three thousand vacancy hops, well below the total number of almost twenty trillion different vacancy structures (including first and second near neighbours). Nevertheless, the results show clearly that diffusion is slower when there is a wide spread of well energies (high σ_w) because vacancies can become trapped in the lowest energy wells, but is faster when there is a wide spread of saddle-point energies (high σ_s) because vacancies can take migration paths that simply avoid the highest energy barriers.

There has been considerable discussion in the previous literature about whether or not diffusion is slower in multicomponent high-entropy solid-solution single phases relative to pure materials,[63–67] somewhat confused by the difficulties of deciding what are appropriate comparison materials, and the complexity of measuring diffusion coefficients from multicomponent material diffusion couples. There is, however, little doubt that diffusion is quite slow in many but not all cases,[3,63,64] often by up to about a half or one order of magnitude, with correspondingly slow diffusion-controlled processes such as precipitation and recrystallisation,[3,16,24] almost certainly caused by the wide variety of local atomic structures as described above. Clearly we need to develop more detailed theories of diffusion in multicomponent high-entropy solid-solution materials such as the fcc Cantor and bcc Senkov alloys, based on non-Fickian atomic percolation through complex structural landscapes with varying lattice-point and saddle-point energies.

11.2 Dislocations and slip

Plastic flow, fracture toughness and formability in crystalline materials are controlled largely by the way in which dislocations move under the action of an applied stress. There is an excess energy per unit length of a dislocation ΔE_d, arising partly from the displacement of atoms along the dislocation line itself, *i.e.* in the dislocation core, and partly from smaller atomic displacements outside the core. The excess energy per unit length or line tension of a dislocation ΔE_d is given by:[35,68,69]

$$E_d = E_c + \frac{\alpha G b^2}{4\pi} \ln \frac{R}{r_c} \approx G b^2$$

where E_c and r_c are the energy and radius of the highly distorted dislocation core region, G is the shear modulus, R is the dislocation spacing, the factor $\alpha = 1$ or $1 - \nu$ for screw or edge dislocations respectively, and ν is Poisson's ratio. In most single-component crystalline materials, the dislocation energy is high and dislocations are difficult to create and immobile, so the materials are hard but brittle, with little plasticity, fracture toughness or formability. In single-component close-packed metals, however, the dislocation energy is much lower and dislocations are relatively easy to create and move,[35,68,69] so the materials are much softer but are ductile, tough (fracture resistant) and formable, with dislocation motion preventing the build-up of local high stresses and cracking.[35,68,69] The overall flow stress τ required to move a dislocation can usually be treated as a straightforward sum of different contributions to the material strength:[1,2]

$$\Delta\tau = \tau_o + \tau_{wh} + \tau_{ss} + \tau_{gb} + \tau_{ph}$$

where τ_o is the lattice friction stress, and τ_{wh}, τ_{ss}, τ_{gb} and τ_{ph} are strengthening contributions from work hardening, solution hardening, grain boundaries and precipitates respectively.

Dislocation motion in a concentrated multicomponent high-entropy solid-solution such as an fcc Cantor alloy or a bcc Senkov alloy is more complex, because of the wide variety of different local atomic structures and associated lattice distortions surrounding atoms along the length of the core of a dislocation[3,44] (as discussed previously and as shown in Tables 6 and 7 and Fig. 9 and 10), and a correspondingly wide variation in the dislocation core energy and line tension E_c and ΔE_d. The atomic structure varies widely from point to point along a dislocation line, and also from time to time at any given point on a dislocation line as it moves under the action of an applied stress.[3,44] Once again, we have not yet made much experimental or theoretical progress towards developing a detailed understanding of this complex range of different local dislocation structures, the resulting dislocation motions and interactions, and, therefore, the overall plasticity in multicomponent high-entropy materials.

Dislocations in fcc Cantor alloys are in some ways found to be similar to those observed previously in pure fcc metals and dilute fcc binary alloys with a relatively low stacking fault energy.[70–72] Unlike pure fcc metals and dilute binary fcc alloys, however, the dislocations in multicomponent single-phase fcc Cantor alloys are wavy rather than straight on a near-atomic scale, with a wide variation along the dislocation line in the separation of the two Shockley partials (and, therefore, the

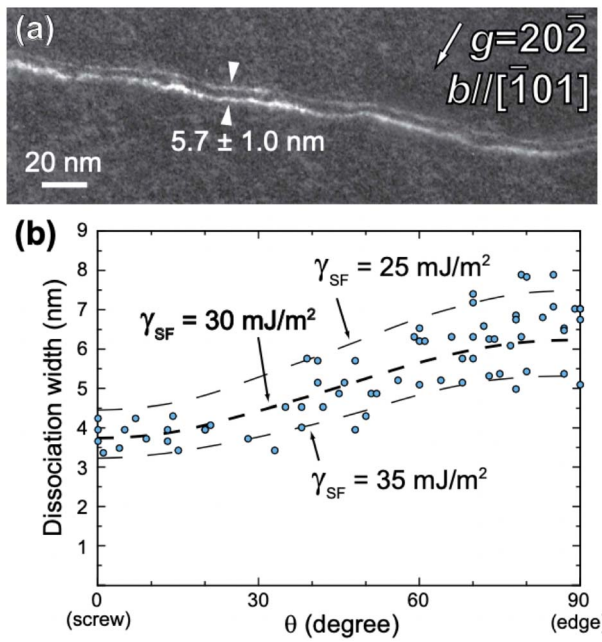

Fig. 13 (a) High-resolution weak-beam image of a $\frac{1}{2}\langle 110\rangle$ dislocation in the original fcc Cantor alloy CrMnFeCoNi showing a wavy dislocation line and separation into two $\frac{1}{6}\langle 112\rangle$ Shockley partials; and (b) partial separation distance d in a large number of dislocations as a function of dislocation orientation θ, ranging from pure screw ($\theta = 0°$) to pure edge ($\theta = 90°$) (after Okamoto *et al.*[73]).

width of the stacking fault between them and corresponding stacking fault energy), and a much higher shear stress needed for slip along the {111} planes.[70–76] An example of a wavy dislocation and measurements of the varying partial separation and corresponding stacking fault energy[73] are shown in Fig. 13 for the original fcc Cantor alloy CrMnFeCoNi. These effects are all caused by the variation in local atomic structures along the dislocation lines as described above, with the associated local lattice strains acting as pinning centres for the dislocations. Okamoto *et al.*[73] used high-resolution weak-beam imaging to make a large number of measurements of the separation between partials along the length of dislocation lines in the original fcc Cantor alloy CrMnFeCoNi, which were found to be variable in the range $d = 3$–8 nm, corresponding to stacking fault energies in the range $\gamma_{sf} = 25$–35 mJ m^{-2}. Similar wavy dislocations with varying separation of partials along the dislocation line have also been seen in a number of multicomponent single-phase fcc Cantor alloys using a variety of transmission electron microscope techniques and also *via* atomistic *ab initio* modelling techniques.[74–79]

Dislocation structures in bcc Senkov alloys are also found to be similar in some ways to those observed previously in pure bcc metals and dilute bcc binary alloys.[80–83] Unlike pure bcc metals and dilute binary bcc alloys, however, the dislocations in multicomponent single-phase bcc Senkov alloys are, like the fcc Cantor alloys, wavy rather than straight on a near-atomic scale, and require a much higher shear stress for slip along the different planes.[80–83] These effects are again, like the fcc Cantor alloys, caused by the variation in local atomic structures along the dislocation lines, with the associated local lattice strains acting as pinning centres for the dislocations.

There has been some success in explaining the strength of multicomponent high-entropy solid-solution materials such as the fcc Cantor alloys and bcc Senkov alloys, based on averaging the pinning effects of varying local atomic structures along the dislocation lines.[84–89] Clearly, we still need to investigate experimentally what must be a much wider range of varying dislocation behaviour, and thus develop a more detailed theory of overall dislocation dynamics, as dislocations move about and interact within a complex landscape of varying local atomic structure and associated varying dislocation energies.

As already mentioned, a much higher shear stress is needed for dislocation slip in multicomponent high-entropy solid-solution single-phase materials such as the fcc Cantor alloys and bcc Senkov alloys. This is caused by the variation in local atomic structures along the dislocation lines, with the associated local lattice strains acting as pinning centres for the dislocations.[3,44] Effectively this corresponds to raising the lattice friction stress because of the dense number of pinning centres created by a high concentration of many different types of solute atoms. The shear flow stress can be rewritten as:[3,44]

$$\begin{aligned}\tau &= \tau_o + \tau_{wh} + \tau_{ss} + \tau_{gb} + \tau_{ph}\\ &\approx \tau_o + \tau_{wh} + \tau_{gb}\\ &\approx \tau_o + 2\alpha G b \rho^{1/2} + \beta d^{-1/2}\end{aligned}$$

where τ_{ph} is taken as zero in a material with no precipitates; the solid-solution strengthening τ_{ss} is incorporated into an enhanced lattice friction stress τ_o; work hardening is given by a Taylor parabolic variation with dislocation density ρ, *i.e.* $\tau_{wh} \approx 2\alpha G b \rho^{\frac{1}{2}}$, where α is a constant, G is the shear modulus, and b is the

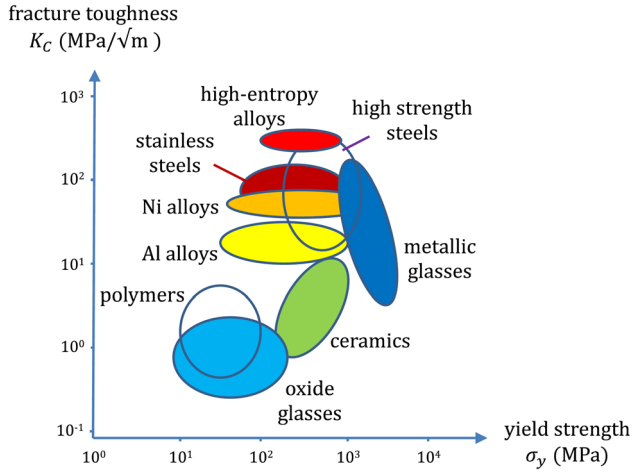

Fig. 14 Schematic Ashby map of fracture toughness K_c *versus* yield strength σ_y for multicomponent high-entropy alloys compared with high-strength steels, nickel superalloys, hard ceramics, and metallic and oxide glasses (redrawn[14] from Gludovatz *et al.*[90] and Li *et al.*[91]).

Burgers vector; and grain-boundary hardening is given by a Hall–Petch variation with grain size d, *i.e.* $\tau_{gb} = \beta d^{-\frac{1}{2}}$, where β is another constant. Overall, this means that multicomponent fcc Cantor alloys and bcc Senkov alloys have outstanding combinations of strength and ductility, as shown in the Ashby map[90] in Fig. 14. According to Li *et al.*:[91] "the CrMnFeCoNi alloy represents one of the toughest materials reported to date, with a plane-strain fracture toughness, K_{1c}, that exceeds 200 MPa/$\sqrt{m}$ and with an outstanding tensile strength exceeding 1 GPa". Much research is now underway to improve even further the mechanical properties of these multicomponent high-entropy materials *via* additional strengthening mechanisms such as reducing the grain size, work hardening *via* severe plastic deformation, and alloying to develop precipitation hardening.[3,16,44,91–98]

11.3 Grain boundaries and recrystallisation

There is a wide range of grain boundaries with a correspondingly wide range of complex structures and energies, even in pure materials and simple alloys.[46,68] Not surprisingly, the complexity of grain-boundary structures is much greater still in multicomponent high-entropy materials. The topological structural complexity of accommodating atomic and molecular sites midway between two differently oriented crystals is compounded in a concentrated multicomponent high-entropy solid-solution, such as an fcc Cantor alloy or a bcc Senkov alloy, by the additional compositional complexity of accommodating a large number of different component atoms across the various grain-boundary sites.[3,44] In any polycrystalline Cantor or Senkov alloy, the enormous variety of different local atomic clusters, such as shown in Fig. 6 and 7 and Tables 9 and 10, has to be distributed across the many different grain-boundary sites all along the many different grain-boundary planes.[3,44] The resulting complexity and multiplicity of grain boundary structures in multicomponent high-entropy solid-solution single-phase materials

are, of course, similar to the complexity and multiplicity discussed previously, arising in the same way for vacancy and dislocation structures in these materials.[3,44]

Direct observation of grain-boundary structures is not easy, even in pure materials and simple dilute binary alloys, because of the complex imaging conditions created by the atomic or molecular disorganisation in grain-boundary regions,[46,68] complicating the use of standard high-resolution imaging techniques such as transmission electron microscopy (TEM), X-ray diffraction (XRD) and atom probe tomography (AP). And the problems associated with the direct observation of grain-boundary structures are only made worse by the chemical complexity found in multicomponent high-entropy materials. Not surprisingly, therefore, there have been relatively few attempts to investigate multicomponent high-entropy grain-boundary structures by direct observation,[3,16,99] and there have also been relatively few attempts to use atomistic modelling techniques,[3,16,100–102] which are more straightforward technically, but always suffer, as remarked previously, from not being able to handle anywhere near the very large number of different local atomic clusters that are present in multicomponent high-entropy materials.

A common method of controlling grain size is by using a mixture of deformation and heat treatment to homogenise and then recrystallise the material.[103,104] There have been quite a few studies of recrystallisation, grain growth and texture in the original equiatomic five-component single-phase fcc Cantor alloy CrMnFeCoNi[105–111] and its equiatomic single-phase fcc quaternary (CrFeCoNi, MnFeCoNi and CrMnCoNi) and ternary (CrFeNi, CrCoNi, MnFeNi, MnCoNi and FeCoNi) subsystems.[110,112–114] Recrystallisation and grain growth in these multicomponent materials are found to be considerably slower than in fcc pure metals and binary alloys, essentially caused by the wide range of local atomic structures and corresponding lattice strains, as shown in Fig. 6 and Table 9, slowing the rates of atomic diffusion during heat treatment.[105–107,110,113] Recrystallisation temperatures correspond typically to homologous temperatures relative to the melting point of $T_r/T_m = 0.6$–0.75, depending on the alloy composition and the extent of deformation,[113] considerably higher than the more typical values in conventional pure metals and binary alloys of $T_r/T_m = 0.3$–0.5. The resulting final recrystallised grain sizes are, as a consequence, very small and slow to coarsen, often no larger than 1–5 μm after 1 hour at annealing temperatures of 700–800 °C (973–1073 K)[105–107,110,113] and much smaller than found in fcc nickel,[114] independent of the extent of the initial deformation treatment.[105–107,110,113]

11.4 Surfaces and catalysis

Like grain boundaries, the local atomic structure at the surface of a material and the corresponding surface energy depend in a complicated way on the crystallography, orientation and topography of the surface.[1,2] Many important processes and corresponding properties of a material, such as for instance wear, oxidation, corrosion and catalysis, depend intrinsically on its exposure to the external environment and are controlled, therefore, by the details of the variety of local atomic structures at its external surfaces. These processes and associated properties are, not surprisingly, fairly complex even in relatively simple single-phase single-component pure materials[1,2] and, also not surprisingly, become much

more complex again in multicomponent high-entropy materials, because of the enormous variety of different local atomic structures,[3,44] as shown in Fig. 6 and 7 and Tables 9 and 10. The variety of different atomic structures across the surface of concentrated multicomponent high-entropy metallic and ceramic materials has been shown to lead to considerable enhancements in catalytic efficiency for many different chemical reactions taking place at the surfaces of a variety of different multicomponent high-entropy materials.[115–118] As an example of multicomponent metallic catalysis, five-component FeCoPdIrPt nanoparticles on graphene oxide (FeCoPdIrPt/GO) were shown by Gao *et al.*[119] to operate at a much lower overvoltage yet with 26 times greater catalytic efficiency for the hydrogen evolution reaction (HER) in a solution of one molar potassium hydroxide (KOH), compared with either single, binary or ternary nanoparticles (such as Fe/GO, CoPd/GO or PdIrPt/GO) or conventional platinised graphite Pt/C. As an example of multicomponent ceramic catalysis, Okejiri *et al.*[120] used $Ru_{0.13}$(-BaSrBi)(ZrHfTiFe)O_3 nanoparticles as catalysts for the conversion of CO to CO_2 and achieved faster conversion at lower temperatures compared with $BaRuO_3$, even though it contains a much higher concentration of ruthenium.

12. What is the electronic structure of high-entropy materials?

In multicomponent high-entropy materials, there are wide and extensive variations in local atomic structure leading to correspondingly wide and extensive variations in local mechanical strain in the lattice.[3,44] And, as just discussed in the previous section, these variations in local mechanical strain affect many important properties, including atomic diffusion and resistance to degradation, dislocation slip and the resulting combination of strength and plasticity, grain boundary motion and recrystallisation, and surface reactivity and catalysis.[3,44] Variations in local mechanical strain are, not surprisingly, mirrored by similar variations in local electronic strain.[3,44] The electronic structure of multicomponent high-entropy materials is, of course, distorted and strained for just the same basic reason as their mechanical structure is distorted and strained, *i.e.* because of the wide and extensive variations in local atomic structure discussed previously, so that the density of electronic states is not the same at all points throughout the lattice.[3,44]

All of our understanding of the electronic behaviour of crystalline materials comes from being able to find approximate solutions to the time-dependent Schrödinger equation:[121–123]

$$i\hbar\frac{\partial\Psi}{\partial t} = \mathscr{H}\Psi$$

where††† $i = \sqrt{-1}$, $\hbar = h/2\pi$, h is Planck's constant, $\Psi(\boldsymbol{r_i})$ is the wave function for the set of constituent fundamental particles (electrons, protons and neutrons) i at positions $\boldsymbol{r_i}$ in the material, E is the energy of the atom and $\mathscr{H} = \mathcal{T} + \nu$ is the Hamiltonian given by:

††† Notice that i in the exponential is the imaginary number: $i = \sqrt{-1}$, and that elsewhere i is a label for different electrons: $\{i\} = i, j, k$, *etc.*

$$\mathscr{H} = \mathcal{T} + \nu = -\sum_i \frac{\hbar^2}{2m_i}\nabla_i{}^2 + \frac{1}{2}\sum_{i\neq j}\frac{e^2}{4\pi\varepsilon_o}\frac{z_i z_j}{(\boldsymbol{r_i} - \boldsymbol{r_j})}$$

where $\mathcal{T}$ and ν are kinetic and potential energy operators given respectively on the right-hand side by the sum of the individual kinetic energies of all the constituent fundamental particles i and the sum of the individual electrostatic attractions or repulsions of all pairs of constituent fundamental particles i and j, m_i and $\boldsymbol{r_i}$ are the mass and position of the i'th particle, e is the charge on the electron, $z_i = -1$, +1 and 0 for electrons, protons and neutrons, respectively, and $\nabla_i{}^2 = \partial/\partial x_i{}^2 + \partial/\partial y_i{}^2 + \partial/\partial z_i{}^2$ is the Laplacian operator for the i'th particle. Solving this equation requires a large number of simplifying approximations,[121–123] including the following: concentrating on stationary states to remove time-dependence, *i.e.* solving the simpler time-independent (instead of time-dependent) Schrödinger equation $E\Psi = \mathscr{H}(\Psi)$;[122,123] using the Born–Oppenheimer approximation[124] to concentrate on the valence electrons only, by assuming the nucleus and inner electrons of each atom form a relatively massive clamped central ion that is effectively fixed in space; using the Hohenberg–Kohn theorem[125] to concentrate exclusively on the ground state of the electrons, with the energy a function then of the electron density $\rho(\boldsymbol{r})$ rather than the set of all electron positions $\{\boldsymbol{r_i}\}$, which is why the methodology is often called density functional theory (DFT); treating the valence electrons as independent by re-writing the overall wave function $\Psi(\boldsymbol{r_i}) = \prod_i \psi_i(\boldsymbol{r_i})$, *i.e.* as a product of a set of individual wave functions $\psi_i(\boldsymbol{r_i})$, one for each valence electron i;[122,123] and using Bloch's theorem,[126] to re-write further the set of wave functions $\psi_i(\boldsymbol{r_i})$ as a simpler set of plane waves $\phi_i(\boldsymbol{r_i}) = \mathrm{e}^{i\boldsymbol{k}\boldsymbol{r}_i}$ modulated by a function $u_i(\boldsymbol{r_i}) = u_i(\boldsymbol{r_i} + \boldsymbol{R})$ which has the periodicity of the crystal lattice:

$$\psi_i(\boldsymbol{r_i}) = \phi_i(\boldsymbol{r_i})u_i(\boldsymbol{r_i}) = \mathrm{e}^{i\boldsymbol{k}\boldsymbol{r}_i}u_i(\boldsymbol{r_i})$$

where $\boldsymbol{k}$ is the wave vector and $\boldsymbol{R}$ is any symmetry operation in the crystal lattice. The Bloch theorem[126] enables the stationary set of plane wave functions for the valence electrons to be determined and described within a Brillouin zone that is characteristic of the material and is identical around each atom at each lattice point. Unfortunately, the variation in local atomic structure in multicomponent high-entropy materials disrupts the periodicity of the crystal structure sufficiently to invalidate Bloch's theorem.[3,44] Essentially, the electronic structure, the Brillouin zone and the density of electronic states are all varying so much from lattice site to lattice site that a plane-wave solution to Schrödinger's equation is not realistic.

The mechanical strains in multicomponent high-entropy materials act as pinning points, making atomic diffusion difficult by restricting vacancy migration and dislocation slip. Similarly, the electronic strains in multicomponent high-entropy materials act as scattering points, making electronic motion difficult and leading to relatively low electrical conductivity.[3,44,127–133] Because of the disruption of lattice periodicity described above, it is very difficult to determine more complex electronic behaviour, and we clearly need more experimental and theoretical studies to explore the resulting electronic, optical and magnetic properties.

13. How can we explore multicomponent phase space?

All the early attempts to explore multicomponent phase space and discover new and exciting multicomponent and high entropy materials were undertaken using traditional *ad hoc* investigation methods, *i.e.* they were pure discovery science, driven largely by trial and error. There have been many attempts since then to use more structured approaches, underpinned by more fundamental scientific theories, and aimed at providing *ab initio* predictions of multicomponent material structures and properties.[3,16,18,134,135] Unfortunately, however, although these attempts have often provided useful information, they have nevertheless been no more than partially successful, mainly because of the enormity of multicomponent phase space and the complexity of the multicomponent materials within it.[3,16,18,134,135] Because of the vast size of multicomponent phase space, we have still only studied relatively few of the trillions of multicomponent materials within it, so our databank of information is quite sparse. And because of the compositional complexity of multicomponent high-entropy materials, our best scientific modelling techniques, even when supported by high-performance computers, are unable to cope adequately with the resulting wide-ranging and extensive variation of local nanostructures contained within them.

The techniques that have been employed to explore multicomponent phase space have included the following: semi-empirical multicomponent Hume-Rothery rules;[3,16,18,134–136] thermodynamic (Calphad) modelling;[3,16,18,137–140] atomistic modelling using density functional theory (DFT), molecular dynamics (MD) and Monte-Carlo (MC) methods;[3,16,18,123,141] and statistical machine-learning (ML) algorithms such as support vector machines, decision trees and neural networks.[3,16,18,142–147] Overall, there has been, therefore, quite a large number of detailed studies using multicomponent Hume-Rothery rules,[148–162] thermodynamic modelling,[163–172] atomistic modelling[173–194] and machine learning,[195–212] all aiming to predict the structures and properties of a variety of different multicomponent and high-entropy materials. In summary, all this work shows that valuable information can be obtained, but that the results are somewhat variable and not in general sufficiently accurate for reliable *ab initio* predictions of either the structures or properties of new multicomponent and high-entropy materials. Hume-Rothery methods try to correlate material structures with parameters calculated from the atomic radii, valencies, electronegativities, bulk modulii, melting points and enthalpies and entropies of the component atomic species.[3,16,18,134–136] There are, not surprisingly, clear but rough correlations, with solid solutions being favoured for materials where the components have similar values of atomic radius, valency and electronegativity, and where the heats of mixing are small and the entropies of mixing are large, but the results are not good enough to guarantee that *ab initio* predictions are correct.[3,18] Calphad-style thermodynamic modelling is based on the fundamental equation discussed previously for the Gibbs free energy of a material:[3,16,18,137–140]

$$G = \sum_i x_i \mu_i^{ss} = \sum_i x_i \mu_i + \Delta G_{mix}$$

$$= \sum_i x_i \mu_i + \Delta H_{mix}(\omega_{ij}, \psi_{ijk}, \chi_{ijkl} \ldots) + RT \sum_i x_i \ln x_i - T \Delta S_{mix}^{xs}(\omega_{ij}, \psi_{ijk}, \chi_{ijkl} \ldots)$$

The Gibbs free energy can, in most cases, be calculated only by using estimates for the set of interaction energies ω_{ij}, ψ_{ijk}, χ_{ijkl}… *etc.* that are effectively obtained by extrapolating from known binary mixtures of materials, and this often misses important non-linearities in the behaviour of the large numbers of concentrated and interacting solutes that are present in multicomponent materials. As with multicomponent Hume-Rothery rules, therefore, thermodynamic modelling calculations are helpful but not sufficient to make *ab initio* predictions without first conducting a detailed experimental study of the region of multicomponent phase space of interest.[3,18] Atomistic modelling studies using density functional theory, molecular dynamics or Monte Carlo methods[3,16,18,123,141] perform quantum mechanical, classical mechanical or probabilistic calculations, respectively, to determine the behaviour of a relatively small number of atoms as a basic calculation unit that is repeated periodically in space. Approximate methods are used to try to build a suitable basic calculation unit that is representative of the material, but it inevitably has far too few atoms to come anywhere near representing the millions of different local nanostructures that are present in multicomponent high-entropy materials, as discussed previously. As with multicomponent Hume-Rothery rules and thermodynamic modelling, therefore, the results are again helpful but insufficient to guarantee successful *ab initio* prediction of structures and properties.[3,18] Machine-learning methods can also be useful,[3,16,18,142–147] but are again somewhat limited and not guaranteed to give good *ab initio* predictions, in this case because they work essentially by discovering patterns in existing data, and are, therefore, successful at interpolating to predict new information within a known range of materials, but not really successful at extrapolating to predict new information in previously unexplored regions of multicomponent phase space.[3,18] Overall, therefore, we can conclude that, in order to achieve successful exploration of multicomponent phase space, there is at present no real alternative to detailed experimental investigation, though this can often be helpfully guided by initial use of multicomponent Hume-Rothery rules, thermodynamic and atomistic modelling and machine-learning calculations.[3,18]

14. Conclusions

After a decade and a half of intensive scientific investigation, we have established that multicomponent phase space is very large and contains an enormous number of new materials that have never been made before. Many multicomponent materials are also high-entropy materials, *i.e.* single-phase solid solutions with random or near-random multiple occupancy of all the lattice sites or one or more of the sublattice sites in the crystal structure. High-entropy materials are based on well-known single-component and binary (and sometimes ternary) compound crystal structures, each with many different compositions, and each occupying a large and complex single-phase field in multicomponent phase space. Increasing the number of components in a material beyond two or three leads to multicomponent high-entropy solid-solution versions of existing single-component and binary and ternary compound structures, rather than the development of entirely new multicomponent compound structures with multiple sublattices. The solid-solution single-phase fields in multicomponent phase space are separated by similarly large and complex multiple-phase fields. Some high-entropy materials have been studied intensively, but most have not, and only a few multiple-phase

materials have been studied so far. We have not yet mapped out in any detail the extent of the different single-phase and multiple-phase fields. High-entropy materials exhibit large variations in local atomic nanostructure, extending over large distances in the crystal structure, leading to similarly large variations in local mechanical and electronic strain in the lattice. Variations in mechanical strain make it difficult for defects such as vacancies, dislocations and grain boundaries to move around in the high-entropy materials, enhancing their resistance to degradation by exposure to high temperatures, irradiation and corrosion, and increasing their strengths without compromising fracture toughness. We need to develop more detailed experimental and theoretical understanding of the behavior of defects such as vacancies, dislocations, grain boundaries and surfaces within complex multicomponent landscapes of varying local atomic structures and energies in order to explain more fully many of the important thermal and mechanical properties of high-entropy materials. Variations in electronic strain act as scattering centres and make it difficult for electrons to move around, reducing the overall electrical conductivity of high-entropy materials. We need similarly to develop more detailed experimental and theoretical understanding of the behaviour of electrons within complex multicomponent landscapes of varying local atomic structures and energies to explain more fully many of the important electrical, optical and magnetic properties of high-entropy materials. We also need more detailed investigation of the wide variety of different multicomponent multiphase materials. The enormous size of multicomponent phase space and the wide range and extent of different local nanostructures that are present in multicomponent high-entropy materials make it difficult to use thermodynamic modelling, atomistic modelling or machine learning-methods with any certainty of successful prediction of new multicomponent high-entropy materials without associated detailed experimental investigation.

Conflicts of interest

The author has no conflicts of interest. He received laboratory and office support from the Department of Materials, University of Oxford and Brunel Centre for Advanced Casting Technology (BCAST), Brunel University London.

Data availability

No primary research results, software or code have been included and no new data were generated or analysed as part of this manuscript.

Acknowledgements

The author wishes to thank the Department of Materials at the University of Oxford and the Brunel Centre for Advanced Solidification Technology (BCAST) at Brunel University London for the provision of laboratory and office facilities.

References

1 M. F. Ashby, D. R. H. Jones, *Engineering Materials*, Pergamon, Oxford, 1986.
2 J. W. Martin, *Materials for Engineering*, Institute of Materials, London, 1996.

3 B. Cantor, *The Fundamentals of Multicomponent High-Entropy Materials*, Oxford University Press, Oxford, 2024.
4 B. Cantor, I. T. H. Chang, P. Knight and A. J. B. Vincent, Microstructural development in equiatomic multicomponent alloys, *Mater. Sci. Eng.*, 2004, **375**, 213–218.
5 A. J. B. Vincent, A study of three multicomponent alloys, Undergraduate thesis, University of Sussex, 1981.
6 B. Cantor, K. B. Kim and P. J. Warren, Novel multicomponent amorphous alloys, *Mater. Sci. Forum*, 2002, **386–388**, 27–32.
7 K. B. Kim, P. J. Warren and B. Cantor, Formation of metallic glasses in novel (Ti33Zr33Hf33)((100-x-y)(Ni50Cu50)(x)Al(y) alloys, *Mater. Trans.*, 2003, **44**, 411–413.
8 K. B. Kim, P. J. Warren and B. Cantor, Metallic glass formation in multicomponent (Ti, Zr, Hf, Nb)-(Ni, Cu, Ag)-Al alloys, *J. Non-Cryst. Solids*, 2003, **317**, 17–22.
9 K. B. Kim, Y. Zhang, P. J. Warren and B. Cantor, Crystallization behaviour in a new multicomponent TiZrHfNiCuAl metallic glass developed by the equiatomic substitution technique, *Philos. Mag.*, 2003, **83**, 2371–2381.
10 P. K. Huang, J. W. Yeh, T. T. Shun and S. K. Chen, Multi-principal-element alloys with improved oxidation and wear resistance for thermal spray coating, *Adv. Eng. Mater.*, 2004, **6**, 74–78.
11 J. W. Yeh, S. K. Chen, S. J. Lin, J. Y. Gan, T. S. Chin, T. T. Shun, C. H. Tsau and S. Y. Chang, Nanostructured high entropy alloys with multiple principal elements: novel alloy design concepts and outcomes, *Adv. Eng. Mater.*, 2004, **6**, 299–303.
12 J. W. Yeh, S. K. Chen, J. Y. Gan, S. J. Lin, T. S. Chin, T. T. Shun, C. H. Tsau and S. Y. Chang, Formation of simple crystal structures in Cu-Co-Ni-Cr-Al-Fe-Ti-V alloys with multiprincipal metallic elements, *Metall. Mater. Trans.*, 2004, **35**, 2533–2536.
13 C. Y. Hsu, J. W. Yeh, S. K. Chen and T. T. Shun, Wear resistance and high-temperature compression strength of fcc $Al_{0.5}$CrFeNiCoCu alloy with boron additions, *Metall. Mater. Trans.*, 2004, **35**, 1465–1469.
14 B. Cantor, The discovery and significance of multicomponent high-entropy alloys, in *Fundamental Studies of High-Entropy Materials*, ed. J. Brechtl and P. K. Liaw, Springer, New York, 2021, ch. 1.
15 J. W. Yeh, My trip from physics to high entropy materials, in *Fundamental Studies of High-Entropy Materials*, ed. J. Brechtl and P. K. Liaw, Springer, New York, 2021, ch. 2.
16 B. S. Murty, J. W. Yeh, S. Ranganathan and P. P. Bhattacharjee, *High-entropy Alloys*, Elsevier, Amsterdam, 2nd edn, 2019.
17 J. Brechtl and P. K. Liaw, *Fundamental Studies of High-Entropy Materials*, ed. J. Brechtl and P. K. Liaw, Springer, New York, 2021.
18 B. Cantor, Exploring multicomponent phase space to discover new materials, *J. Phase Equilib. Diffus.*, 2024, **45**, 188–218.
19 *Worldwide Guide to Equivalent Irons and Steels*, ed. F. Cverna, ASM International, Materials Park, Ohio, 5th edn, 2006.
20 *Worldwide Guide to Equivalent Non-ferrous Metals and Alloys*, ed. F. Cverna, ASM International, Materials Park, Ohio, 4th edn, 2001.

21 *Annual Book of ASTM Standards*, ASTM International, West Conshohocken, Pennsylvania, 2020.
22 K. M. Koh and C. C. Chen, *Principles and Techniques in Combinatorics*, World Scientific, Singapore, 1992.
23 R. A. Brualdi, *Introductory Combinatorics*, Pearson Prentice Hall, Hoboken, NJ, 5th edn, 2010.
24 B. Cantor, Multicomponent high-entropy Cantor alloys, *Prog. Mater. Sci.*, 2021, 100754.
25 O. N. Senkov, G. B. Wilks, D. B. Miracle, C. P. Chuang and P. K. Liaw, Refractory high-entropy alloys, *Intermetallics*, 2010, **18**, 1758–1765.
26 O. N. Senkov, D. B. Miracle and K. J. Chaput, Development and exploration of refractory high entropy alloys — a review, *J. Mater. Res.*, 2018, **33**, 3092–3218.
27 D. B. Miracle, M. H. Tsai, O. N. Senkov, V. Soni and R. Banerjee, Refractory high entropy superalloys, *Scr. Mater.*, 2020, **187**, 445–452.
28 *Copper and Copper Alloys*, ed. J. R. Davis, ASM International, Materials Park, Ohio, 2001.
29 H. K. D. H. Bhadeshia and R. W. K. Honeycombe, *Steels: Microstructure and Properties*, Butterworth-Heinemann, Oxford, 4th edn, 2017.
30 J. D. Musgraves, J. Hu and L. Calvez, *Springer Handbook of Glass*, Springer-Nature, Switzerland, 2019.
31 C. R. M. Grovenor, *Microelectronic Materials*, Adam Hilger, Bristol, 1989.
32 L. Mondolfo, *Aluminium Alloys: Structure and Properties*, Architectural Press, Taylor and Francis, Oxford, 2nd edn, 1979.
33 D. R. Gaskell and D. E. Laughlin, *Introduction to the Thermodynamics of Materials*, CRC Press, Boca Raton, 6th edn, 2017.
34 M. Hillert, *Phase Equilibria, Phase Diagrams and Phase Transformations*, Cambridge University Press, Cambridge, 2nd edn, 2008.
35 B. Cantor, *The Equations of Materials*, Oxford University Press, Oxford, 2020.
36 B. Cantor, The thermodynamics of multicomponent high-entropy materials, *J. Mater. Sci.*, 2024, **60**, 1750–1764.
37 E. J. Pickering, R. Muñoz-Moreno, H. J. Stone and N. G. Jones, Precipitation in the equiatomic high-entropy alloy CrMnFeCoNi, *Scr. Mater.*, 2016, **113**, 106–109.
38 F. Otto, A. Diouhý, K. G. Pradeep, M. Kuběnovà, D. Raabe, G. Eggeler and E. P. George, Decomposition of the single-phase high-entropy alloy CrMnFeCoNi after prolonged anneals at intermediate temperatures, *Acta Mater.*, 2016, **112**, 40–52.
39 J. M. Cowley, An approximate theory of order in alloys, *Phys. Rev.*, 1950, **77**, 669–675.
40 M. Laurent-Brocq, A. Akhatova, L. Perrière, S. Chebini, X. Sauvage and E. Leroy, Insights into the phase diagram of the CrMnFeCoNi high entropy alloy, *Acta Mater.*, 2015, **88**, 355–365.
41 C. M. Rost, E. Sachet, T. Borman, A. Moballegh, F. C. Dickey, D. Hou, J. L. Jones, S. Curtarolo and J.-P. Maria, Entropy-stabilized oxides, *Nat. Commun.*, 2015, **6**, 8485.
42 R. Zhang, S. Zhao, J. Ding, Y. Chong, T. Jia, C. Ophus, M. Asta, R. O. Ritchie and A. M. Minor, Short-range order and its impact on the CoCrNi medium-entropy alloy, *Nature*, 2020, **581**, 283–287.

43 S. Maiti and W. Steurer, Structural disorder and its effect on mechanical properties in single-phase TaNbHfZr high-entropy alloy, *Acta Mater.*, 2016, **106**, 87–97.
44 B. Cantor, Local nanostructure in multicomponent high-entropy materials, *High Entropy Alloys and Materials*, 2024, **2**, 277–306.
45 F. C. Philips, *An Introduction to Crystallography*, Wiley, New York, 1973.
46 A. Kelly and K. M. Knowles, *Crystallography and Crystal Defects*, Wiley, New York, 2012.
47 N. N. Greenwood and A. Earnshaw, *Chemistry of the Elements*, Butterworth-Heinemann, Oxford, 2nd edn, 1997.
48 N. L. Okamoto, K. Yuge, K. Tanaka, H. Inui and E. P. George, Atomic Displacement in the CrMnFeCoNi High Entropy Alloy: A Scaling Factor to Predict Solid Solution Strengthening, *AIP Adv.*, 2016, **6**, 125008.
49 H. S. Oh, D. Ma, G. P. Leyson, B. Grabowski, E. S. Park, F. Körmann and D. Raabe, Lattice distortions in the FeCoNiCrMn high entropy alloy studied by theory and experiment, *Entropy*, 2016, **18**, 321–329.
50 H. Song, F. Tian, Q. M. Hu, L. Vitos, Y. Wang, J. Shen and N. Chen, Local lattice distortions in high-entropy alloys, *Phys. Rev. Mater.*, 2018, **1**, 023404.
51 C. C. Yen, G. R. Huang, Y. C. Huang, H. W. Yeh, D. J. Luo, K. T. Hsieh, E. W. Huang, J. W. Yeh, S. J. Lin, C. C. Wang, C. L. Kuo, S. Y. Chang and Y. C. Lo, Lattice distortion effect on elastic anisotropy of high entropy alloys, *J. Alloys Compd.*, 2020, **818**, 152876.
52 L. R. Owen, E. J. Pickering, H. Y. Playford, H. J. Stone, M. G. Tucker and N. G. Jones, An assessment of the lattice strain in the CrMnFeCoNi high-entropy alloy, *Acta Mater.*, 2017, **122**, 11–18.
53 Y. Y. Tan, M. Y. Su, Z. C. Xie, Z. J. Chen, Y. Gong, L. R. Zheng, Z. Shi, G. Mo, Y. Li, L. W. Li, H. Y. Wang and L. H. Dai, Chemical composition dependent local lattice distortions and magnetism in high entropy alloys, *Intermetallics*, 2021, **129**, 107050.
54 Y. Tong, K. Jin, H. Bei, J. Y. P. Ko, D. C. Pagan, Y. Zhang and F. X. Zhang, Local lattice distortion in NiCoCr, FeCoNiCr and FeCoNiCrMn concentrated alloys investigated by synchrotron X-ray diffraction, *Mater. Des.*, 2018, **155**, 1–7.
55 Y. Tong, S. Zhao, K. Jin, H. Bei, J. P. Y. Ko, Y. Zhang and F. X. Zhang, A comparison study of local lattice distortion in $Ni_{80}Pd_{20}$ binary alloy and FeCoNiCrPd high entropy alloy, *Scr. Mater.*, 2018, **156**, 14–18.
56 H. Ge and F. Tian, A review of ab initio calculation on lattice distortion in high-entropy alloys, *J. Met.*, 2019, **71**, 4225–4237.
57 Y. Zou, S. Maiti, W. Steurer and R. Spolenak, Size-dependent plasticity in an $Nb_{25}Mo_{25}TA_{25}W_{25}$ refractory high-entropy alloy, *Acta Mater.*, 2014, **65**, 85–97.
58 W. Guo, W. Dmowski, J. Y. Noh, P. Rack, P. K. Liaw and T. Egami, Local atomic structure of a high-entropy alloy: an X-ray and neutron scattering study, *Metall. Mater. Trans.*, 2013, **44**, 1994–1997.
59 S. Maiti and W. Steurer, Structural disorder and its effect on mechanical properties in single-phase TaNbHfZr high-entropy alloy, *Acta Mater.*, 2016, **106**, 87–97.
60 R. Abbaschian, L. Abbaschian and R. E. Reed-Hill, *Physical Metallurgy Principles*, Nelson Engineering, 4th edn, 2009.
61 P. Shewmon, *Diffusion in Solids*, Springer, New York, 2nd edn, 2016.

62 S. L. Thomas and S. Patala, Vacancy diffusion in multi-principal element alloys: the role of chemical disorder in the ordered lattice, *Acta Mater.*, 2020, **196**, 144–153.
63 K. Y. Tsai, M. H. Tsai and J. W. Yeh, Sluggish diffusion in CoCrFeMnNi high-entropy alloy, *Acta Mater.*, 2013, **61**, 4887–4897.
64 M. Vaidya, K. G. Pradeep, B. S. Murty, G. Wilde and S. V. Divinsky, Bulk tracer diffusion in CoCrFeNi and CoCrFeMnNi high entropy alloys, *Acta Mater.*, 2018, **146**, 211–224.
65 M. Vaidya, S. Trubel, B. S. Murty, G. Wilde and S. V. Divinsky, Ni tracer diffusion in CoCrFeNi and CoCrFeMnNi high entropy alloys, *J. Alloys Compd.*, 2016, **688**, 994–1001.
66 Q. Li, W. Chen, J. Zhong, L. Zhang, Q. Chen and Z. Liu, On sluggish diffusion in fcc AlCoCrFeNi high-entropy alloys: an experimental and numerical study, *Metals*, 2018, **8**, 16.
67 J. Dabrowa and M. Danielewsky, State-of-the-art diffusion studies in the high entropy alloys, *Metals*, 2020, **10**, 347–391.
68 W. Cai and W. D. Nix, *Imperfections in Crystalline Solids*, Cambridge University Press, Cambridge, 2016.
69 D. Hull and D. J. Bacon, *Introduction to Dislocations*, Butterworth-Heinemann, Elsevier, Oxford, 5th edn, 2011.
70 Z. Li, S. Zhao, R. O. Ritchie and M. A. Meyers, Mechanical properties of high-entropy alloys with emphasis on face-centered cubic alloys, *Prog. Mater. Sci.*, 2019, **102**, 296–345.
71 E. P. George, W. A. Curtin and C. C. Tasan, High entropy alloys: A focused review of mechanical properties and deformation mechanisms, *Acta Mater.*, 2020, **188**, 435–474.
72 W. Li, D. Xie, D. Li, Y. Zhang, Y. Gao and P. K. Liaw, Mechanical behaviour of high-entropy alloys, *Prog. Mater. Sci.*, 2021, **118**, 100777.
73 N. L. Okamoto, S. Fujimoto, Y. Kambara, M. Kawamura, Z. M. T. Chen, H. Matsunoshita, K. Tanaka, H. Inui and E. P. George, Size effect, critical resolved shear stress, stacking fault energy, and solid solution strengthening in the CrMnFeCoNi high-entropy alloy, *Nature Sci. Rep.*, 2016, **6**, 35863.
74 T. M. Smith, M. S. Hooshmand, B. D. Esser, F. Otto, D. W. McComb, E. P. George, M. Ghazisaeidi and M. J. Mills, Atomic-scale characterization and modelling of 60° dislocations in a high-entropy alloy, *Acta Mater.*, 2016, **110**, 352–363.
75 G. Laplanche, A. Kostka, C. Reinhart, J. Hunfeld, G. Eggeler and E. P. George, Reasons for the superior mechanical properties of medium-entropy CrCoNi compared to high-entropy CrMnFeCoNi, *Acta Mater.*, 2017, **128**, 292–303.
76 X. D. Xu, P. Liu, Z. Tang, A. Hirata, S. X. Song, T. G. Nieh, P. K. Liaw, C. T. Liu and M. W. Chen, Transmission electron microscopy characterization of dislocation structure in a face-centred cubic high-entropy alloy $Al_{0.1}$CoCrFeNi, *Acta Mater.*, 2018, **144**, 107–115.
77 R. Pasianot and D. Farkas, Atomistic modeling of dislocations in a random quinary high-entropy alloy, *Comput. Mater. Sci.*, 2020, **173**, 109366.
78 S. I. Rao, C. Woodward, T. A. Parthasarathy and O. N. Senkov, Atomistic simulations of dislocation behaviour in a model fcc multicomponent concentrated solid solution alloy, *Acta Mater.*, 2017, **134**, 188–194.

79 X. Liu, Z. Pei and M. Eisenbach, Dislocation core structures and Peierls stresses of the high entropy alloy NiCoFeCrMn and its subsystems, *Mater. Des.*, 2019, **180**, 107955.
80 J. P. Couzinie, L. Lilensten, Y. Champion, G. Dirras, L. Perrière and I. Guillot, On the room temperature deformation mechanisms of a TiZrHfNmMo refractory high-entropy alloy, *Mater. Sci. Eng.*, 2015, **645**, 255–263.
81 L. Lilensten, J. P. Couzinie, L. Perrière, A. Hocini, C. Keller, G. Dirras and I. Guillot, Study of a bcc multi-principal element alloy: tensile and simple shear properties and underlying deformation mechanism, *Acta Mater.*, 2018, **142**, 131–141.
82 F. Wang, G. H. Balbus, S. Xu, Y. Su, J. Shin, P. F. Rottmann, K. E. Knipling, J. C. Stinville, L. H. Mills, O. N. Senkov, I. J. Beyerlein, T. M. Pollock and D. S. Gianola, Multiplicity of dislocation pathways in a refractory multiprincipal element alloy, *Science*, 2020, **370**, 95–101.
83 C. Lee, F. Maresca, R. Feng, Y. Chou, T. Ungar, M. Widom, K. An, J. D. Poplawsky, Y. C. Chou, P. K. Liaw and W. A. Curtin, Strength can be controlled by edge dislocations in refractory high-entropy alloys, *Nat. Commun.*, 2021, 5474.
84 C. Varvenne, A. Luque and W. A. Curtin, Theory of strengthening in fcc high entropy alloys, *Acta Mater.*, 2016, **118**, 164–176.
85 C. Varvenne, G. P. M. Leyson, M. Ghazisaeidi and W. A. Curtin, Solute strengthening in random alloys, *Acta Mater.*, 2017, **124**, 660–683.
86 C. Varvenne and W. A. Curtin, Strengthening of high entropy alloys by dilute solute additions: CoCrFeNiAlx and CoCrFeNiMnAlx alloys, *Scr. Mater.*, 2017, **138**, 92–95.
87 S. Sohn, Y. Liu, J. Liu, P. Gong, S. Prades-Rodel, A. Blatter, B. E. Scanlon, C. C. Broadbridge and J. Schroers, Noble metal high entropy alloys, *Scr. Mater.*, 2017, **126**, 29–32.
88 B. Yin and W. A. Curtin, First-principles-based prediction of yield strength in the RhIrPdPtNiCu high-entropy alloy, *npj Comput. Mater.*, 2019, **5**, 14.
89 F. Maresca and W. A. Curtin, Theory of screw dislocation strengthening in random bcc alloys from dilute to high-entropy alloys, *Acta Mater.*, 2020, **182**, 144–162.
90 B. Gludovatz, A. Hohenwarter, D. Catoor, E. H. Chang, E. P. George and R. O. Ritchie, A fracture-resistant high-entropy alloy for cryogenic applications, *Science*, 2014, **345**, 1153–1158.
91 Z. Li, S. Zhao, R. O. Ritchie and M. A. Meyers, Mechanical properties of high-entropy alloys with emphasis on face-centered cubic alloys, *Prog. Mater. Sci.*, 2019, **102**, 296–345.
92 E. P. George, W. A. Curtin and C. C. Tasan, High entropy alloys: A focused review of mechanical properties and deformation mechanisms, *Acta Mater.*, 2020, **188**, 435–474.
93 W. Li, D. Xie, D. Li, Y. Zhang, Y. Gao and P. K. Liaw, Mechanical behaviour of high-entropy alloys, *Prog. Mater. Sci.*, 2021, **118**, 100777.
94 O. N. Senkov, D. B. Miracle, K. J. Chaput and J. P. Couzinie, Development and exploration of refractory high entropy alloys – a review, *J. Mater. Res.*, 2018, **33**, 3092–3128.
95 D. B. Miracle, M. H. Tsai, O. N. Senkov, V. Soni and R. Banerjee, Refractory high entropy superalloys, *Scr. Mater.*, 2020, **187**, 445–452.

96 J. Zhou, Y. Cheng, Y. Chen and X. Liang, Composition design and preparation process of refractory high-entropy alloys: a review, *Int. J. Refract. Metals Hard Mater.*, 2022, **105**, 105836.
97 X. Ren, Y. Li, Y. Qi and B. Wang, Review on preparation technology and properties of refractory high entropy alloys, *Materials*, 2022, **15**, 2931.
98 B. Chen and L. Zhuo, Latest progress on refractory high entropy alloys: composition, fabrication, post processing, performance, simulation and prospect, *Int. J. Refract. Metals Hard Mater.*, 2023, **110**, 105993.
99 Q. Lin, X. An, H. Liu, Q. Tang, P. Dai and X. Liao, In-situ high-resolution transmission electron microscopy investigation of grain boundary dislocation activities in a nanocrystalline CrMnFeCoNi high-entropy alloy, *J. Alloys Compd.*, 2017, **709**, 802–807.
100 P. Wynblatt and D. Chatain, Modeling grain boundary and surface segregation in multicomponent high-entropy alloys, *Phys. Rev. Mater.*, 2019, **3**, 054004.
101 D. Farkas, Grain boundary structure in high-entropy alloys, *J. Mater. Sci.*, 2020, **55**, 9173–9183.
102 H. Lee, M. Shabani, G. J. Pataky and F. Abdeljawad, Tensile deformation behavior of twist grain boundaries in CoCrFeMnNi high entropy bicrystals, *Nature Sci. Rep.*, 2021, **11**, 428.
103 R. D. Doherty, D. A. Hughes, F. J. Humphreys, J. J. Jonas, D. J. Jensen, M. E. Kassner, W. E. King, T. R. McNelley, H. J. McQueen and A. D. Rollett, Current issues in recrystallization: a review, *Mater. Sci. Eng.*, 1997, **238**, 219–274.
104 J. Humphreys, G. S. Rohrer and A. Rollett, *Recrystallization and Related Annealing Phenomena*, Elsevier, Amsterdam, 3rd edn, 2017.
105 W. H. Liu, Y. Wu, J. Y. He, T. G. Nieh and Z. P. Lu, Grain growth and the Hall-Petch relationship in a high-entropy FeCrNiCoMn alloy, *Scr. Mater.*, 2013, **68**, 526–529.
106 P. P. Bhattacharjee, G. D. Sathiaraj, M. Zaid, J. R. Gatti, C. Lee, C. W. Tsai and J. Y. Yeh, Microstructure and texture evolution during annealing of equiatomic CoCrFeMnNi high-entropy alloy, *J. Alloys Compd.*, 2014, **587**, 544–552.
107 F. Otto, N. L. Hanold and E. P. George, Microstructural evolution after thermomechanical processing in an equiatomic single-phase CoCrFeMnNi high-entropy alloy with special focus on twin boundaries, *Intermetallics*, 2014, **54**, 39–48.
108 G. Laplanche, O. Horst, G. Eggeler and E. P. George, Microstructural evolution of a CoCrFeMnNi alloy after swaging and annealing, *J. Alloys Compd.*, 2015, **647**, 548–557.
109 G. D. Sathiaraj and P. P. Bhattacharjee, Analysis of microstructure and microtexture during grain growth in low stacking fault energy equiatomic CoCrFeMnNi high entropy and Ni-60wt%Co alloys, *J. Alloys Compd.*, 2015, **637**, 267–276.
110 B. R. Chen, A. C. Yeh and J. W. Yeh, Effect of one-step recrystallization on the grain boundary evolution of CoCrFeMnNi high entropy alloy and its subsystems, *Nature Sci. Rep.*, 2016, **6**, 22306.
111 J. Gu, S. Ni, Y. Liu and M. Song, Regulating the strength and ductility of a cold rolled FeCrCoMnNi high-entropy alloy via annealing treatment, *Mater. Sci. Eng.*, 2019, **755**, 289–294.

112 P. Shiyamoorthi, P. Asghari-Rad, J. W. Bae and H. S. Kim, Fine tuning of tensile properties in CrCoNi medium entropy alloy through cold rolling and annealing, *Intermetallics*, 2019, **113**, 106578.
113 Z. Wu, H. Bei, F. Otto, G. M. Pharr and E. P. George, Recovery, recrystallization, grain growth and phase stability of a family of fcc-structured multicomponent equiatomic solid solution alloys, *Intermetallics*, 2014, **46**, 131–140.
114 Z. Yang, F. He, Q. Wu, K. Zhang, D. Cui, B. Guo, B. Han, J. Li, J. Wang and Z. Wang, Distinct recrystallization kinetics in NiCoCrFe-based single-phase high-entropy alloys, *Metall. Mater. Trans.*, 2021, **52**, 3799–3810.
115 Y. Zhang, D. Wang and S. Wang, High-entropy alloys for electrocatalysis: design, characterization and applications, *Small*, 2022, **18**, 2104339.
116 K. Kusada, M. Mukoyoshi, D. Wu and H. Kitagawa, Chemical synthesis, characterization and properties of multi-element nanoparticles, *Angew. Chem.*, 2022, **61**, 09616.
117 H. Li, J. Lai, Z. Li and L. Wang, Multi-sites electrocatalysis in high-entropy alloys, *Adv. Funct. Mater.*, 2021, **31**, 2106715.
118 B. Wang, Y. Yao, X. Yu, C. Wang, C. Wu and Z. Zou, High entropy alloys: from theory to experiment, *J. Mater. Chem. A*, 2021, **9**, 19410–19438.
119 S. Gao, S. Hao, Z. Huang, Y. Yuan, S. Han, L. Lei, X. Zhang, R. Shahbazian-Yassar and J. Lu, Synthesis of high-entropy alloy nanoparticles on supports by the fast moving bed pyrolysis, *Nat. Commun.*, 2020, **11**, 2016.
120 F. Okejiri, Z. Zhang, J. Liu, M. Liu, S. Yang and S. Dai, Room-temperature synthesis of high-entropy perovskite oxide nanoparticle catalysts through ultrasonication-based method, *ChemSusChem*, 2019, **13**, 111–115.
121 C. Kittel, *Introduction to Solid State Physics*, Wiley, New York, 2nd edn, 1957.
122 A. P. Sutton, *Electronic Structure of Materials*, Oxford University Press, Oxford, 1993.
123 *Introduction to Materials Modelling*, ed. Z. H. Barber, Maney, London, 2005.
124 M. Born and R. Oppenheimer, Zur quantentheorie der molekeln [On the quantum theory of molecules], *Ann. Phys.*, 1927, **84**, 457–484.
125 P. Hohenberg and W. Kohn, Inhomogeneous electron gas, *Phys. Rev. [Sect.] B*, 1964, **136**, 864–871.
126 F. Bloch, Über die quantenmechanik der elektronen in kristalgittern [On the quantum mechanics of electrons in crystal lattices], *Z. Phys.*, 1928, **52**, 555–600.
127 P. Bag, Y. C. Su, Y. K. Kuo, Y. C. Lai and S. K. Wu, Physical properties of face-centred cubic structured high-entropy alloys: effects of NiCo, NiFe and NiCoFe alloying with Mn, Cr and Pd, *Phys. Rev. Mater.*, 2021, **5**, 085003.
128 G. D. Samolyuk, S. Mu, A. F. May, B. C. Sales, S. Wimmer, S. Mankovsky, H. Ebert and G. M. Stocks, Temperature-dependent electronic transport in concentrated solid solutions of the 3d-transition metals Ni, Fe, Co and Cr from first principles, *Phys. Rev. B*, 2018, **98**, 165141.
129 S. Mu, G. D. Samolyuk, S. Wimmer, M. C. Troparevsky, S. Khan, S. Mankovsky, H. Ebert and G. M. Stocks, Uncovering electron scattering mechanisms in NiFeCoCrMn derived concentrated solid solution and high entropy alloys, *npj Comput. Mater.*, 2019, **5**, 1–8.
130 K. Jin, B. C. Sales, G. M. Stocks, G. D. Samolyuk, M. Daene, W. J. Weber, Y. Zhang and H. Bei, Tailoring the physical properties of Ni-based single-

phase equiatomic alloys by modifying the chemical complexity, *Sci. Rep.*, 2016, **6**, 20159.

131 Y. Mu, H. Liu, Y. Liu, X. Zhang, Y. Jiang and T. Dong, An ab initio and experimental studies of the structure, mechanical parameters and state density on the refractory high-entropy alloy systems, *J. Alloys Compd.*, 2017, **714**, 668–680.

132 C. Chang and H. Zhang, First-principles calculations to investigate elastic and thermodynamic properties of $FeAlNi_xCrMn$ quinternary alloys, *J. Mater. Res. Technol.*, 2022, **18**, 1322–1332.

133 Y. Tong, L. Bai, X. Liang, Y. Chen, Z. Zhang, J. Liu, Y. Li and Y. Hu, Influence of alloying elements on mechanical and electronic properties of NbMoTaWX (X = Cr, Zr, V, Hf and Re) refractory high entropy alloys, *Intermetallics*, 2020, **126**, 106928.

134 D. B. Miracle and O. N. Senkov, A critical review of high-entropy alloys and related concepts, *Acta Mater.*, 2017, **122**, 448–511.

135 V. K. Soni, S. Sanyal, K. Raja Rao and S. K. Sinha, A review on phase prediction in high entropy alloys, *J. Mech. Eng. Sci.*, 2021, **235**, 6268–6286.

136 U. Mizutani, *Hume-Rothery Rules for Structurally Complex Alloy Phases*, CRC Press, Boca Raton, 2019.

137 C. Li, Y. Yuan, F. Li, Q. Wei and Y. Huang, Modification and verification of Miedema model for predicting thermodynamic properties of binary precipitates in multi-element alloys, *Phys. B*, 2022, **627**, 413540.

138 L. Kaufman and H. Bernstein, *Computer Calculations of Phase Diagrams*, Academic Press, New York, 1970.

139 N. Saunders and A. P. Miodownik, *Calphad: Calculation of Phase Diagrams: A Comprehensive Guide*, Pergamon Elsevier, Oxford, 1998.

140 H. L. Lukas, S. G. Fries and B. Sundman, *Computational Thermodynamics*, Cambridge University Press, Cambridge, 2007.

141 F. Giustino, *Materials Modelling Using Density Functional Theory*, Oxford University Press, Oxford, 2014.

142 L. Qiao, Y. Liu and J. Zhu, A focused review on machine learning aided high-throughput methods in high entropy alloy, *J. Alloys Compd.*, 2021, **877**, 160295.

143 G. L. W. Hart, T. Mueller, C. Toher and S. Curtarolo, Machine learning for alloys, *Nat. Rev. Mater.*, 2021, **6**, 730–755.

144 X. Liu, P. Xu, J. Zhao, W. Lu, M. Li and G. Wang, Material machine learning for alloys: applications, challenges and perspectives, *J. Alloys Compd.*, 2022, **921**, 165984.

145 A. Burkov, *The Hundred Page Machine Learning Book*, ed. A. Burkov, 2019.

146 P. Flach, *Machine Learning: the Art and Science of Algorithms that Make Sense of Data*, Cambridge University Press, Cambridge, 2012.

147 S. Russell and P. Norvig, Section V: Machine Learning, in *Artificial Intelligence: A Modern Approach*, Pearson Education, Harlow, 4th edn, 2022, pp. 669–873.

148 Y. Zhang, Y. J. Zhou, J. P. Lin, G. L. Chen and P. K. Liaw, Solid-solution phase formation rules for multi-component alloys, *Adv. Eng. Mater.*, 2008, **10**, 534–538.

149 X. Yang and Y. Zhang, Prediction of high-entropy stabilized solid-solution in multi-component alloys, *Mater. Chem. Phys.*, 2012, **132**, 233–238.

150 Y. Zhang, X. Yang and P. K. Liaw, Alloy design and properties optimization of high-entropy alloys, *J. Met.*, 2012, **64**, 830–838.

151 S. Guo, Q. Hu, C. Ng and C. T. Liu, More than entropy in high-entropy alloys: forming solid solutions or amorphous phase, *Intermetallics*, 2013, **41**, 96–103.
152 A. Takeuchi, K. Amiya, T. Wada, K. Yubuta, W. Zhanb and A. Makino, Entropies in alloy design for high entropy and bulk glassy alloys, *Entropy*, 2013, **15**, 3810–3821.
153 M. X. Ren, B. X. Li and H. Z. Fu, Formation condition of solid solution type high-entropy alloy, *Trans. Nonferrous Met. Soc. China*, 2013, **23**, 991–995.
154 M. G. Poletti and L. Battezzati, Electronic and thermodynamic criteria for the occurrence of high entropy alloys in metallic systems, *Acta Mater.*, 2014, **75**, 297–306.
155 G. A. Salishchev, M. A. Tikhonovsky, D. G. Shaysultanov, N. D. Stepanov, A. V. Kuznetsov, I. V. Kolodiy, A. S. Tortika and O. N. Senkov, Effect of Mn and V on structure and mechanical properties of high-entropy alloys based on CoCr- FeNi system, *J. Alloys Compd.*, 2014, **591**, 11–21.
156 Z. S. Nong, J. C. Zhu, Y. Cao, X. W. Yang, Z. H. Lai and Y. Liu, Stability and structure prediction of cubic phase in as cast high entropy alloys, *Mater. Sci. Technol.*, 2014, **30**, 363–369.
157 S. Guo, Phase selection rules for cast high entropy alloys: an overview, *Mater. Sci. Technol.*, 2015, **31**, 1223–1230.
158 Z. Wang, Y. Huang, Y. Yang, J. Wang and C. T. Liu, Atomic size effect and solid solubility of multicomponent alloys, *Scr. Mater.*, 2015, **94**, 28–31.
159 Y. F. Ye, Q. Wang, J. Lu, C. T. Liu and Y. Yang, The generalized thermodynamic rule for phase selection in multicomponent alloys, *Intermetallics*, 2015, **59**, 75–80.
160 D. J. M. King, S. C. Middleburgh, A. G. Mc Gregor and M. B. Cortie, Predicting the formation and stability of single phase high-entropy alloys, *Acta Mater.*, 2016, **104**, 172–179.
161 O. N. Senkov and D. B. Miracle, A new thermodynamic parameter to to predict formation of solid solutions or intermetallic phases in high entropy alloys, *J. Alloys Compd.*, 2016, **658**, 603–607.
162 I. T. Caraballo and P. E. J. Rivera-Diaz-del-Castillo, A criterion for the formation of high entropy alloys based on lattice distortion, *Intermetallics*, 2016, **71**, 76–87.
163 K. C. Hsieh, C. F. Yu, W. T. Hsieh, W. R. Chiang, J. S. Ku, J. H. Lai, C. P. Tu and C. C. Yang, The microstructure and phase equilibrium of new high performance high-entropy alloys, *J. Alloys Compd.*, 2009, **483**, 209–212.
164 C. Huang, Y. Zhang, J. Shen and R. Vilar, Thermal stability and oxidation resistance of laser clad TiVCrAlSi high entropy alloy coatings on Ti-6Al-4V alloy, *Surf. Coat. Technol.*, 2011, **206**, 1389–1395.
165 O. N. Senkov, F. Zhang and J. D. Miller, Phase composition of a CrMoNbTaTiZr high entropy alloy:comparison of experimental and simulated data, *Entropy*, 2013, **15**, 3796–3809.
166 M. C. Gao and D. E. Alman, Searching for next single-phase high-entropy alloy compositions, *Entropy*, 2013, **15**, 4504–4519.
167 J. E. Saal, I. S. Berglund, J. T. Sebastian, P. K. Liaw and G. B. Olson, Equilibrium high entropy alloy phase stability from experiments and thermodynamic modeling, *Scr. Mater.*, 2018, **146**, 5–8.
168 T. T. Shun and Y. C. Du, Microstructure and tensile behaviors of fcc $Al_{0.3}$CoCrFeNi high entropy alloy, *J. Alloys Compd.*, 2009, **479**, 157–160.

169 Y. F. Kao, S. K. Chen, T. J. Chen, P. C. Chu, J. W. Yeh and S. J. Lin, Electrical, magnetic and Hall properties of $Al_xCoCrFeNi$ high-entropy alloys, *J. Alloys Compd.*, 2011, **509**, 1607–1614.

170 W. R. Wang, W. L. Wang and J. W. Yeh, Phases, microstructure and mechanical properties of $Al_xCoCrFeNi$ high-entropy alloys at elevated temperatures, *J. Alloys Compd.*, 2014, **589**, 143–152.

171 Q. Tang, Y. Huang, H. Cheng, X. Liao, T. G. Langdon and P. Dai, The effect of grain size on the annealing-induced phase transformation in an $Al_{0.3}CoCrFeNi$ high entropy alloy, *Mater. Des.*, 2016, **105**, 381–385.

172 F. He, Z. Wang, Q. Wu, J. Li, J. Wang and C. T. Liu, Phase separation of metastable CoCrFeNi high entropy alloy at intermediate temperatures, *Scr. Mater.*, 2017, **126**, 15–19.

173 F. Tian, A review of solid-solution models of high-entropy alloys based on ab initio calculations, *Front. Mater.*, 2017, **4**, 36.

174 F. Tian, Y. Wang, D. L. Irving and L. Vitos, Applications of coherent potential approximations to HEAs, in *High-Entropy Alloys: Fundamentals and Applications*, ed. M. C. Gao, J. W. Yeh, P. K. Liaw and Y. Zhang, Springer International, Switzerland, 2016, ch. 9, pp. 299–332.

175 M. C. Gao, C. Niu, C. Jiang and D. L. Irving, Applications of special quasi-random structures to high-entropy alloys, in *High-Entropy Alloys: Fundamentals and Applications*, ed. M. C. Gao, J. W. Yeh, P. K. Liaw and Y. Zhang, Springer International, Switzerland, 2016, ch. 10, pp. 333–368.

176 D. Ma, B. Grabowski, F. Körmann, J. Neugebauer and D. Raabe, Ab initio thermodynamics of the CoCrFeMnNi high entropy alloy: importance of entropy contributions beyond the configurational one, *Acta Mater.*, 2015, **100**, 90–97.

177 X. Sun, H. Zhang, S. Lu, X. Ding, Y. Wang and L. Vitos, Phase selection rule for Al-doped CrMnFeCoNi high-entropy alloys from first principles, *Acta Mater.*, 2017, **140**, 366–374.

178 J. Y. He, W. H. Liu, H. Wang, Y. Wu, X. J. Liu, T. G. Nieh and Z. P. Lu, Effects of Al addition on structural evolution and tensile properties of the FeCoNiCrMn high-entropy alloy system, *Acta Mater.*, 2014, **62**, 105–113.

179 F. Y. Tian, L. Delczeg, N. X. Chen, L. K. Varga, J. Shen and L. Vitos, Structural stability of $NiCoFeCrAl_x$ high-entropy alloy from ab initio theory, *Phys. Rev. B: Condens. Matter Mater. Phys.*, 2013, **88**, 085128.

180 S. Yang and Y. Zhong, Ab initio modeling of fcc FeCoCrNi high entropy alloys with full composition range, *J. Phase Equilib. Diffus.*, 2021, **42**, 656–672.

181 S. Yang, G. Liu and Y. Zhong, Revisit the VEC criterion in high entropy alloys (HEAs) with high throughput ab initio calculations: a case study with AlCoCrFeNi system, *J. Alloys Compd.*, 2022, **916**, 165477.

182 S. Guo, C. Ng, J. Lu and C. Liu, Effect of valence electron concentration on stability of fcc or bcc phase in high entropy alloys, *J. Appl. Phys.*, 2011, **109**, 103505.

183 F. Tian, L. K. Varga, N. Chen, J. Shen and L. Vitos, Ab initio design of elastically isotropic $TiZrNbMoV_x$ high-entropy alloys, *J. Alloys Compd.*, 2014, **599**, 19–25.

184 S. W. McAlpine, J. V. Logan and M. P. Short, Predicting single phase stability and segregation in the NbMoTaTi-(W,V) high entropy alloy system with the vacancy exchange potential, *Scr. Mater.*, 2021, **191**, 29–33.

185 Q. Zhao, J. Li, Q. Fang and H. Feng, Effect of Al solute concentration on mechanical properties of Al_xFeCuCrNi high-entropy alloys: a first principles study, *Phys. B*, 2019, **566**, 30–37.
186 C. Niu, A. J. Zaddach, C. C. Koch and D. L. Irving, First principles exploration of near-equiatomic NiFeCrCo high entropy alloys, *J. Alloys Compd.*, 2016, **672**, 510–520.
187 H. Song, F. Tian, Q. M. Hu, L. Vitos, Y. Wang, J. Shen and N. Chen, Local lattice distortion in high-entropy alloys, *Phys. Rev. Mater.*, 2017, **1**, 023404.
188 M. Karabin, W. R. Mondal, A. Östlin, W. G. D. Ho, V. Dobrosavljevic, K. M. Tam, H. Terletska, L. Chioncel, Y. Wang and M. Eisenbach, Ab initio approaches to high-entropy alloys: a comparison of CPA, SQS and supercell methods, *J. Mater. Sci.*, 2022, **57**, 10677–10690.
189 S. M. Chen, Z. J. Ma, S. Qiu, L. J. Zhang, S. Z. Zhang, R. Yang and Q. M. Hu, Phase decomposition and strengthening in HfNbTaTiZr high entropy alloy from first-principles calculations, *Acta Mater.*, 2022, **225**, 117582.
190 F. Biermair, V. I. Razumovskiy and G. Ressel, Influence of alloying on thermodynamic properties of AlCoCrFeNiTi high entropy alloys from DFT calculations, *Comput. Mater. Sci.*, 2022, **202**, 110952.
191 S. San, Y. Tong, H. Bei, B. Kombaiah, Y. Zhang and W. Y. Ching, First-principles calculation of lattice distortion in four single phase high entropy alloys with experimental validation, *Mater. Des.*, 2021, **209**, 110071.
192 S. Liu, P. Cao, D. Y. Lin and F. Tian, Stability of $L2_1$ $(NiM)_2TiAl$ (M=Co, Fe) in high-entropy alloys, *J. Alloys Compd.*, 2018, **764**, 650–655.
193 S. Wang, S. Chen, Y. Jia, H. Hu, H. Huang, Z. Yang, A. Dong, G. Zhu, D. Wang, D. Shu, F. Tian, Y. Dai and B. Sun, Fcc-$L1_2$ ordering transformation in equimolar FeCoNiV multi-principal element alloy, *Mater. Des.*, 2019, **168**, 107648.
194 R. Ryitsev, V. Gaviko, S. Estemirova, E. Sterkhov, L. Cherepanova, D. Yagodin, N. Chtchelkatchev, N. Dubinin and S. Uporov, Laves formation in high entropy alloys, *Metals*, 2021, **11**, 1962.
195 N. Islam, W. Huang and H. L. Zhuang, Machine learning for phase selection in multi-principal element alloys, *Comput. Mater. Sci.*, 2018, **150**, 230–235.
196 R. Bobbili, B. Ramakrishna and V. Madhu, Development of machine learning based models for design of high entropy alloys, *Mater. Technol.*, 2022, **37**, 2046930.
197 W. Huang, P. Martin and H. L. Zhuang, Machine learning phase prediction of high-entropy alloys, *Acta Mater.*, 2019, **169**, 225–236.
198 P. Mandal, A. Choudhury, A. B. Mallick and M. Ghosh, Phase prediction in high entropy alloys by various machine learning modules using thermodynamic and configurational parameters, *Met. Mater. Int.*, 2022, **29**, 38–52.
199 Y. Yan, D. Lu and K. Wang, Accelerated discovery of single-phase refractory high entropy alloys assisted by machine learning, *Comput. Mater. Sci.*, 2021, **199**, 110723.
200 A. E. Nassar and A. M. Mullis, Rapid screening ofhigh entropy alloys using neural networks and constituent elements, *Comput. Mater. Sci.*, 2021, **199**, 110755.
201 K. Kaufmann and K. S. Vecchio, Searching for high entropy alloys: machine learning approach, *Acta Mater.*, 2020, **198**, 178–222.

202 U. K. Jaiswal, Y. V. Krishna, M. R. Rahul and G. Phanikumar, Machine leasrning-enabled identification of new medium to high entropy alloys with solid solution phases, *Comput. Mater. Sci.*, 2021, **197**, 110623.

203 T. Wen, B. Ye, H. Liu, S. Ning, C. Z. Wang and Y. Chu, Formation criteria for binary metal diboride solid solutions established through combinatorial methods, *J. Am. Ceram. Soc.*, 2019, **103**, 3338–3348.

204 K. Kaufmann, D. Maryanovsky, W. M. Mellor, C. Zhu, A. S. Rosengarten, T. J. Harrington, C. Oses, C. Toher, S. Curtarolo and K. S. Vecchio, Discovery of high-entropy ceramics via machine learning, *npj Comput. Mater.*, 2020, **6**, 42.

205 F. Z. Dai, B. Wen, Y. Sun, H. Xiang and Y. Zhou, Theoretical prediction on thermal and mechanicalproperties of high entropy (ZrHfTiNbTa)C by deep learning potential, *J. Mater. Sci. Technol.*, 2020, **43**, 168–174.

206 F. Z. Dai, Y. Sun, B. Wen, H. Xiang and Y. Zhou, Temperature dependent thermal and elastic properties of high entropy (TiZrHfNbTa)B_2: molecular dynamics simulation by deep learning potential, *J. Mater. Sci. Technol.*, 2021, **72**, 8–15.

207 W. M. Mellor, K. Kaufmann, O. F. Dippo, S. D. Figuera, G. D. Schrader and K. S. Vecchio, Development of ultrahigh-entropy ceramics with tailored oxidation behavior, *J. Eur. Ceram. Soc.*, 2021, **41**, 5791–5800.

208 J. Zhang, B. Xu, Y. Xiong, S. Ma, Z. Wang, Z. Wu and S. Zhao, Design high-entropy carbide ceramics from machine learning, *npj Comput. Mater.*, 2022, **8**, 5.

209 R. Mitra, A. Bajpai and K. Biswas, Machine learning based approach for phase prediction in high entropy borides, *Ceram. Int.*, 2022, **48**, 16695–16706.

210 Y. J. Chang, C. Y. Jui, W. J. Lee and A. C. Yeh, Prediction of the composition and hardness of high-entropy alloys by machine learning, *J. Met.*, 2019, **71**, 3433–3442.

211 C. W. Wen, Y. Zhang, C. Wang, D. Xue, Y. Bai, S. Antonav, L. Dai, T. Lookman and Y. Su, Machine learning assisted design of high entropy alloys with desired property, *Acta Mater.*, 2019, **170**, 109–117.

212 C. Wen, C. Wang, Y. Zhang, S. Antonov, D. Xue, T. Lookman and Y. Su, Modeling solid solution strengthening in high entropy alloys using machine learning, *Acta Mater.*, 2021, **212**, 116917.